PCCP

ROYAL SOCIETY OF CHEMISTRY

PERSPECTIVE

View Article Online
View Journal | View Issue

Check for updates

Cite this: *Phys. Chem. Chem. Phys.*, 2022, **24**, 11455

Exploiting the upconversion luminescence, Lewis acid catalytic and photothermal properties of lanthanide-based nanomaterials for chemical and polymerization reactions

Xiangyang Wu* and Edwin K. L. Yeow *

Received 3rd February 2022,
Accepted 12th April 2022

DOI: 10.1039/d2cp00560c

rsc.li/pccp

Lanthanide-based nanocrystals possess three unique physical properties that make them attractive for facilitating photoreactions, namely photon upconversion luminescence, Lewis acid catalytic activity and photothermal properties. When co-doped with a suitable sensitizer and activator lanthanide ions, rare-earth fluoride nanocrystals upconvert near-infrared light to higher energy photons that can be used to excite photosensitizers that absorb ultraviolet and visible light in photocatalytic and photopolymerization reactions. Surface lanthanide ions on nanocrystals also have the propensity to behave as Lewis acid (LA) catalytic sites. In addition, NIR-light excited lanthanides such as Nd^{3+} undergo cross-relaxation interaction with neighbouring ground-state ions followed by non-radiative decay to generate heat (*i.e.*, photothermal) which enhances the rate of chemical reactions. In this perspective, we provide a survey of the recent progress in the use of lanthanide-based nanocrystals as upconverting nanolamps, LA catalysts and photothermal nanoheaters in driving synthetic and polymerization reactions, and the challenges that need to be further addressed in order for this vibrant research area to develop and grow.

Open Access Article. Published on 13 2022. Downloaded on 28.01.2026 17:57:53.
This article is licensed under a Creative Commons Attribution-NonCommercial 3.0 Unported Licence.

1. Introduction

Lanthanides have received enormous attention because of their unique properties such as having rich electronic energy-levels and displaying near infrared (NIR) light-activated Stokes and anti-Stokes emission.[1–12] Lanthanide-doped materials have therefore broadband absorption, downconversion emission from NIR to mid-infrared, and upconversion emission ranging from deep ultraviolet (UV) to visible regions. Lanthanide luminescence arises from f–f electronic transitions within the 4f orbital and is shielded by 5s and 5p orbitals, making lanthanide emission relatively stable.[7,11,13,14] In order to improve emission quantum efficiency, a fluoride-based matrix with low phonon energy is often chosen to host lanthanide dopants (*e.g.*, in lanthanide-based rare-earth metal (Re) fluoride ReF_3 and alkaline (A) Re fluoride ($AReF_4$) nanocrystals).

The photon upconversion properties of (alkaline) Re fluoride nanocrystals allow them to behave as NIR-activated UV/visible 'nanolamps'.[15–22] The emission upconversion nanocrystals (UCNCs) are capable of facilitating a series of important light-induced reactions such as photoisomerization, photopolymerization, photolysis and photocoupling.[7,19–22] The energy of light emitted from UCNCs, covering a wide spectrum range from UV to NIR, can be selectively tuned to excite various photosensitizers. For example, semiconductors excited by

Division of Chemistry and Biological Chemistry, School of Physical and Mathematical Sciences, Nanyang Technological University, 637371, Singapore. E-mail: wuxiangy@ntu.edu.sg, edwinyeow@ntu.edu.sg

Xiangyang Wu received his PhD degree from Nanyang Technological University in 2011 under the supervision of Prof. Edwin K. L. Yeow. He then worked as a research fellow with the same research group. His current research interests include the synthesis and characterization of functional nanomaterials, investigation of the photophysical properties of novel optical materials using both ensemble-averaged and single-molecule fluorescence techniques, and NIR-light activated heterogeneous photocatalysis.

Edwin K. L. Yeow is an Associate Professor of Chemistry at the Nanyang Technological University, Singapore. He is the recipient of the Photochemistry Association Lectureship Award for Asian and Oceanian Photochemist 2018. His research interests include understanding the role and application of light in photoredox catalysis, antimicrobial activity and analytical sensing.

Open Access Article. Published on 13 2022. Downloaded on 28.01.2026 17:57:53.
This article is licensed under a Creative Commons Attribution-NonCommercial 3.0 Unported Licence.

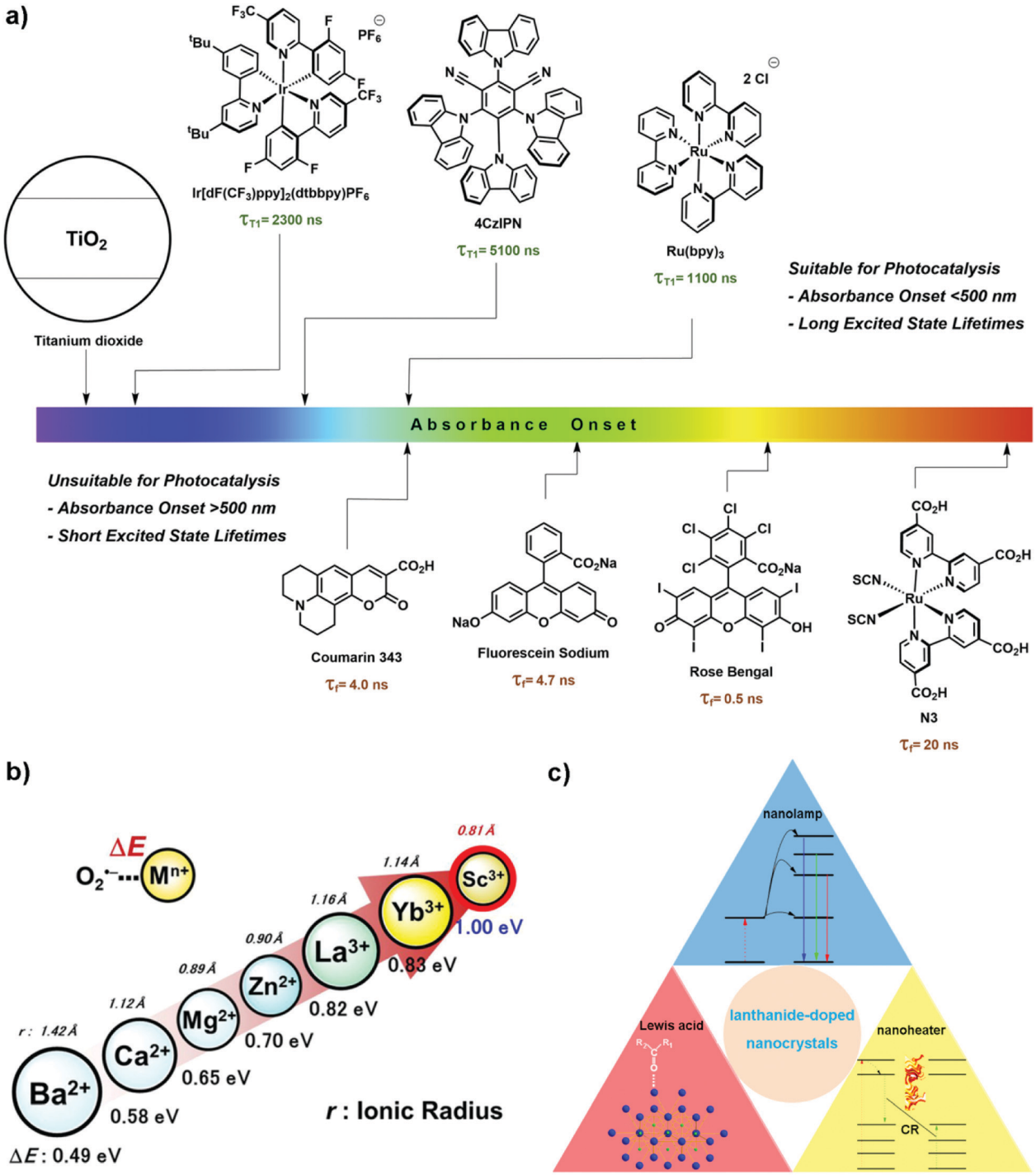

Fig. 1 (a) Absorption window of photosensitizers including dyes and semiconductors.[35] Reprinted with permission from ref. 35. Copyright 2021, Elsevier. (b) The relationship between the Lewis acidity (ΔE) and ionic radius of redox-inactive Re^{3+} ions.[51] Details of the measurement of ΔE can be found in ref. 51. Reprinted with permission from ref. 51. Copyright 2017, Wiley-VCH. (c) Scheme of the three functions (*i.e.*, Lewis acid catalyst, upconversion nanolamp, and photothermal nanoheater) of lanthanide-doped nanocrystals.

upconverted UV photons from UCNCs have been used in water splitting,[6,23,24] wastewater treatment,[6,25–27] nitrogen photofixation[28–30] and photoelectrocatalysis.[6,23,31–34]

To date, most photocatalytic reactions are driven by photoredox catalysts that absorb UV/visible light (Fig. 1a).[35–40] Unfortunately, there are several challenges associated with the utilization of UV/visible light sources: (i) low penetration of UV/visible light in reaction mixtures and opaque reactors, (ii) photodegradation of substrates by direct UV light irradiation, and (iii) competition of the reactants and photocatalysts for the absorption of excitation light; limiting large-scale reactions. NIR light circumvents the above issues since it has good penetration

 This journal is © the Owner Societies 2022

Open Access Article. Published on 13 2022. Downloaded on 28.01.2026 17:57:53.
This article is licensed under a Creative Commons Attribution-NonCommercial 3.0 Unported Licence.

and most reactants do not absorb NIR light.[41,42] Direct excitation of NIR light-absorbing photoredox catalysts such as plasmonic nanoparticles (*e.g.*, Au–Pd[43]), organometallic complexes (*e.g.*, Os(II)-polypyridyl complexes[44]) and organic dyes (*e.g.*, cyanines[45,46]) has been applied in organic synthesis.[47] Alternatively, the use of molecular photon upconversion materials and lanthanide-based UCNCs as internal light sources has been introduced. For example, upconversion photons from NIR-activated triplet–triplet annihilation involving a palladium(II) octabutoxyphthalocyanine sensitizer and a furanyl diketopyrrolopyrrole annihilator are transferred to photoredox catalysts (*e.g.*, Eosin Y, Rose Bengal) needed to drive a series of reactions including hydrodehalogenation, oxidation, radical cyclization, [2+2] cyclization, vinyl azide sensitization and radical polymerization.[42]

Most Re including lanthanides exist in their 3+ oxidation state, except for those with stable 4f configurations (*e.g.*, Ce^{4+}, Tb^{4+}, Eu^{2+} and Yb^{2+}).[48] The electropositive ions act as a Lewis acid (LA) catalyst by accepting electrons from a reactant and increasing its reactivity (*e.g.*, the nucleophilicity of the carbonyl compound).[49] In particular, lanthanides have the propensity to activate double and triple bonds, and coordinate with heteroatoms such as carbonyl oxygen. Compared to other LAs (*e.g.*, Ba^{2+}, Ca^{2+}, Mg^{2+} and Zn^{2+}), the strongly electropositive Re ions are regarded as hard LAs whose Lewis acidity increases with reduced ionic radius (Fig. 1b).[50,51] As such, lanthanide ions have been extensively used as LA catalysts in various organic reactions including aldol reactions, Mannich reactions, cycloaddition reactions, Friedel–Crafts reactions, cyanosilylation and ring opening reactions.[49,52,53]

Photothermal materials (PTMs), capable of converting light into thermal energy, have found useful applications in solar evaporation and photothermal catalysis.[54–56] PTMs including metals (*e.g.*, Au,[57,58] Ag,[59] and Cu[59]), semiconductors,[60,61] carbon materials[62] and polymers[63,64] display efficient light-to-heat conversion efficiency *via* a variety of mechanisms such as plasmonic heating, electron–hole pair relaxation and non-radiative vibrational relaxation. (Alkaline) Re fluoride nanocrystals are also attractive PTMs. The thermal energy generated from these 'nanoheaters' upon NIR light irradiation has been employed in a wide-range of applications such as photothermal therapy,[65–67] anti-counterfeiting technology[68] and nanothermometry.[65,69–72] Unfortunately, lanthanide-based nanomaterials are not widely used in photothermal catalysis despite possessing several advantages over fossil fuels traditionally employed in thermally driven reactions: (i) maximum temperature reached within a short timescale (*e.g.*, down to a few picoseconds) and quick transfer of heat to the environment, (ii) temperature enhancement facilely controlled with a high spatial resolution (*e.g.*, nanometre scale), (iii) use of cumbersome external heating appliances avoided, and (iv) elimination of fossil fuel combustion, hence achieving a greener and more sustainable method of producing heat.[25,54,73]

Given the unique properties of lanthanide-based nanomaterials (*e.g.*, ReF_3 and $AReF_4$) it would be advantageous to exploit their upconversion luminescence, LA catalytic activity and photothermal behaviour to effectively drive organic synthesis and polymerization reactions (Fig. 1c). This perspective introduces previously reported studies relevant to this subject and provides a perspective on its future outlook. Briefly, in Section 2, the working mechanisms and applications of lanthanide-based nanocrystals as NIR-activated 'nanolamps' in photoredox catalysis and photopolymerization will be presented. Photodegradation of organic pollutants will not be included here since it has been well reviewed in ref. 25–27. The role of lanthanide-based nanocrystals as a heterogeneous LA catalyst is discussed in Section 3. This is followed by a discussion on the mechanisms behind their NIR-activated photothermal effect, factors affecting light-to-heat conversion efficiency and applications to reactions. Finally, a short discussion on the challenges faced by ReF_3 and $AReF_4$ nanocrystals as functional heterogeneous catalysts is given.

2. Upconversion nanocrystals

2.1. Photon upconversion

(Alkaline) Re fluoride nanocrystals containing both sensitizer and activator dopants can undergo upconversion luminescence when excited using NIR light. Nd^{3+} and Yb^{3+} with light absorption cross-sections of 1.2×10^{-19} cm^2 at 808 nm and 1.2×10^{-20} cm^2 at 980 nm, respectively, are often employed as the sensitizer, whereas Tm^{3+} and Er^{3+} are common activators.[4,74,75] A core/shell/shell $NaYF_4$:Yb^{3+},Er^{3+}@$NaYF_4$@$NaYF_4$:Nd^{3+},Yb^{3+},Tm^{3+} nanocrystal is used here to illustrate the commonly invoked energy transfer upconversion mechanism (Fig. 2).[76] The effects of using different excitation wavelengths (*i.e.*, 1540, 980 and 808 nm) on the energy of emitted photons are discussed. The $NaYF_4$ shell prevents cross-talk between the emissive $NaYF_4$:Yb^{3+},Er^{3+} core and the $NaYF_4$:Nd^{3+},Yb^{3+},Tm^{3+} shell. Upon 1540 nm light excitation, Er^{3+} ions in the core undergo multiple excited state absorption processes ($^4I_{15/2} \rightarrow {}^4I_{13/2}$, $^4I_{13/2} \rightarrow {}^4I_{9/2}$, $^4I_{9/2} \rightarrow {}^2H_{11/2}$, and $^4I_{11/2} \rightarrow {}^4S_{3/2}$), followed by blue light emission corresponding to the $^2H_{11/2} \rightarrow {}^4I_{15/2}$ and $^4S_{3/2} \rightarrow {}^4I_{15/2}$ transitions and red light emission corresponding to the $^4F_{9/2} \rightarrow {}^4I_{15/2}$ transition.

When an 808 nm excitation light is used instead, non-radiative energy transfer from the excited Nd^{3+} to Yb^{3+} in the outermost shell takes place ($^4F_{3/2}$ (Nd^{3+}) + $^2F_{7/2}$ (Yb^{3+}) $\rightarrow$ $^4I_{9/2}$ (Nd^{3+}) + $^2F_{5/2}$ (Yb^{3+})). The excited Yb^{3+} subsequently transfers its energy to Tm^{3+}, pumping the latter from its $^3H_6$ state to higher energy levels *via* sequential photon absorption:

$$^2F_{5/2}\ (Yb^{3+}) + {}^3H_6\ (Tm^{3+}) \rightarrow {}^2F_{7/2}\ (Yb^{3+}) + {}^3H_5\ (Tm^{3+})$$

$$^2F_{5/2}\ (Yb^{3+}) + {}^3F_4\ (Tm^{3+}) \rightarrow {}^2F_{7/2}\ (Yb^{3+}) + {}^3F_2\ (Tm^{3+})$$

$$^2F_{5/2}\ (Yb^{3+}) + {}^3H_4\ (Tm^{3+}) \rightarrow {}^2F_{7/2}\ (Yb^{3+}) + {}^1G_4\ (Tm^{3+})$$

$$^2F_{5/2}\ (Yb^{3+}) + {}^1G_4\ (Tm^{3+}) \rightarrow {}^2F_{7/2}\ (Yb^{3+}) + {}^1D_2\ (Tm^{3+})$$

The excited Tm^{3+} subsequently emits blue-violet light by the relaxation pathways $^1D_2 \rightarrow {}^3F_4$ and $^1G_4 \rightarrow {}^3H_6$ and red light by $^1G_4 \rightarrow {}^3F_4$.

When a 980 nm excitation light is used to directly excite the Yb^{3+} ions, they can undergo non-radiative energy transfer to

Open Access Article. Published on 13 2022. Downloaded on 28.01.2026 17:57:53.
This article is licensed under a Creative Commons Attribution-NonCommercial 3.0 Unported Licence.

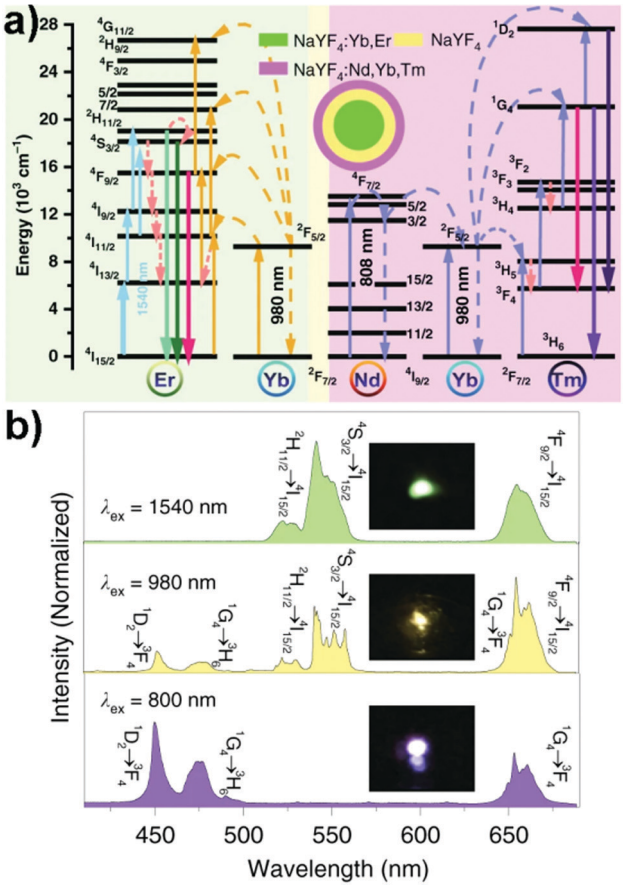

Fig. 2 (a) Proposed multiple excited state absorption and energy transfer mechanism in Nd^{3+}, Yb^{3+}, Er^{3+}, and Tm^{3+}-codoped UCNC.[76] (b) Upconversion emission spectra of UCNCs shown in (a) and the corresponding photo of UCNC films excited using λ_{ex} = 800, 980 and 1540 nm laser excitation.[76] Reprinted with permission from ref. 76. Copyright 2020, Nature Publishing Group.

either Tm^{3+} in the outermost shell or Er^{3+} in the core. Energy transfer from the photoexcited Yb^{3+} to Er^{3+} gives rise to the population of $^2H_{11/2}$, $^4S_{3/2}$ and $^4F_{9/2}$ states which then emit radiatively. The observed yellowish luminescence is thus derived from upconversion emissions from both Tm^{3+} and Er^{3+}. Apart from the energy transfer upconversion mechanism, other explanations used to understand the anti-Stokes shift in emission include excited state absorption, photon avalanche, cooperative upconversion and energy migration-mediated upconversion.[1,6,12,77]

2.2. Photochemical reactions

In 2014, Lee *et al.* performed a NIR-driven photoenzymatic conversion of α-ketoglutarate to L-glutamate using an UCNC-based system involving both photocatalytic and biocatalytic cycles (Fig. 3a).[15] In the former cycle, Rose Bengal (RB) dye molecules, bound onto the surface of a silica shell coated $NaYF_4$:Yb^{3+},Er^{3+} core, were excited by upconverted emission light when irradiated with a 980 nm light. The close proximity between RB and UCNC ensures an efficient Förster resonance energy transfer process. In the latter cycle, photoexcited electrons from RB were transferred to NAD^+ *via* a Rhodium(III)-based mediator (*i.e.*, $[Cp^*Rh(bpy)H_2O]^+$, Cp^* = C_5Me_5, bpy = 2,2′-bipyridine); reducing NAD^+ to NADH (a nicotinamide cofactor) that was needed for the conversion of α-ketoglutarate to L-glutamate in the presence of L-glutamate dehydrogenase. An L-glutamate yield of ~20.25% was achieved when the reaction mixture was exposed to NIR light for 5 h.

Freitag *et al.* designed an NIR-activated photocatalyst containing a heteroleptic $[Ru(bpy)_2L]^{2+}$ complex (*i.e.*, L = 6,6′-([2,2′-bipyridine]-4,4′-diyl)dihexanoic acid) attached onto the surface of $NaYF_4$:Yb^{3+},Tm^{3+} UCNC *via* ligand-exchange (Fig. 3b).[16] Through careful steady-state and time-resolved luminescence studies, the authors proposed that radiative upconverted energy transfer (*i.e.*, trivial energy transfer mechanism) occurred from the excited UCNCs to the bound transition-metal complex which in turn photocatalysed the overall oxidation of ethyl 2-bromo-2-phenylacetate to ethyl 2-oxo-2-phenylacetate under aerobic conditions.

Recently, our group designed an NIR-activated photocatalyst system comprised of Toluidine Blue (TB) molecules bound onto the surface of an UCNC (*i.e.*, $NaYF_4$:Nd^{3+},Yb^{3+},Er^{3+}@$NaYF_4$:Nd^{3+}) (Fig. 3c).[17] Upon light irradiation with an 808 nm light, the excited TB, formed after resonance energy transfer from UCNC, were able to photocatalyze the conversion of dihydrotetrazine (dHTz) to tetrazine. The latter subsequently underwent an inverse electron demand Diels–Alder reaction (IEDDA) with a strained dienophile. This concept was applied to covalently attached a dHTz-vancomycin (Van) antibiotic system to norbornene molecules on bacterial cell walls, and the strategy significantly improved the activity of Van against drug-resistant Enterococci (*i.e.*, MIC was reduced by 6- to 7-fold as compared to neat Van). Wu *et al.* have also labelled sialic acids incorporated into bacterial cells by tetrazole-modified UCNCs *via* photoclick chemistry.[18]

2.3. Photopolymerization

Compared to conventional photopolymerization using direct UV/visible light, UCNC-assisted polymerization has several advantages including easier medical treatment procedures (*e.g.*, treatment of carious lesions), enhanced polymerization rate, improved degree of monomer conversion, and increased polymerization depth.[77–81] The combination of a UCNC and a photoinitiator allows emitted upconverted photons to excite the latter to produce active species that initiate the polymerization reaction. For example, Liu *et al.* performed the polymerization of epoxy acrylate by coupling $NaYF_4$:Yb^{3+},Tm^{3+} UCNC and the photoinitiator Irgacure 784.[81] Due to the deep penetration and weak Rayleigh scattering of NIR excitation light, an impressive curing depth of 13.7 cm was obtained when 0.3 wt% concentration of UCNC was used (Fig. 4a). It is worth noting that the concentration of UCNCs used in the polymerization should be carefully tuned since it significantly affected the degree of monomer conversion and polymerization depth (Fig. 4b).

Another common method for initiating photopolymerization is to generate free radicals using a photosensitizer (*i.e.*, dye)/coinitiator system.[82] Briefly, initiating radicals are produced *via* the following steps (Fig. 4c): (a) an appropriate

 This journal is © the Owner Societies 2022

Open Access Article. Published on 13 2022. Downloaded on 28.01.2026 17:57:53.
This article is licensed under a Creative Commons Attribution-NonCommercial 3.0 Unported Licence.

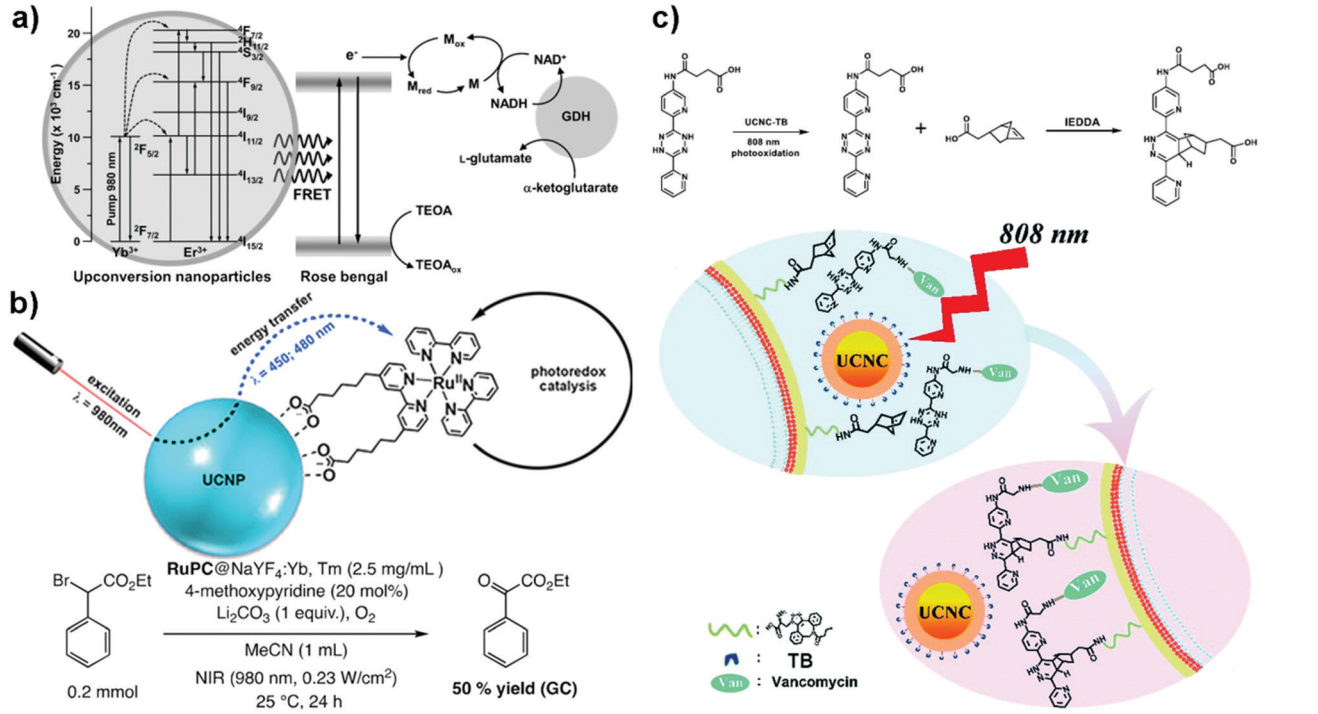

Fig. 3 (a) NIR-driven photoenzymatic catalysts combining $NaYF_4$:Yb^{3+},Er^{3+}, Rose Bengal (RB), a rhodium(III)-based mediator (M), nicotinamide adenine dinucleotide (NAD^+) and L-glutamate dehydrogenase (GDH).[15] Reprinted with permission from ref. 15. Copyright 2014, Wiley-VCH. (b) NIR-driven photocatalyst combining $NaYF_4$:Yb^{3+}, Tm^{3+} and a heteroleptic derivative of $[Ru(bpy)_3]^{2+}$.[16] Reprinted with permission from ref. 16. Copyright 2018, Wiley-VCH. (c) NIR-driven photocatalyst combining $NaYF_4$:Nd^{3+},Yb^{3+},Er^{3+}@$NaYF_4$:Nd^{3+} and Toluidine Blue O (TB).[17] Reprinted with permission from ref. 17. Copyright 2021, Royal Society of Chemistry.

organic dye is first photoexcited, (b) a charge-separated radical-ion pair is formed after electron transfer from the coinitiator (*e.g.*, amines R_2N–CH_2–R′) to the photoexcited dye, (c) a radical pair is formed following proton (H^+) transfer within the radical-ion pair, and (d) radical-pair separation leads to initiating radical generation that (e) reacts with the monomer.

Based on the above mechanism, Xiao *et al.* synthesized poly(ethylene glycol) diacrylate (PEGDA) microspheres using a photoexcited Eosin Y/triethanolamine coinitiator system together with $NaYF_4$:Yb^{3+},Er^{3+} UCNCs as internal lamps.[83] When the UCNC was irradiated with a 980 nm light, upconverted energy was transferred to Eosin Y, inducing the formation of the initiating radicals (Fig. 4d). In addition, lipophilic zinc(II) phthalocyanine (ZnPc) was successfully loaded into the hydrophobic environment of the UCNC-PEGDA hybrid microspheres *via* hydrophobic interaction. In this case, green emission (520 to 554 nm) from the UCNC was used to photoinitiate the polymerisation reaction whereas red emission (640 to 680 nm) was used to photoexcite zinc(II) phthalocyanine to generate $^1O_2$ for photodynamic therapy application.

Beyazit *et al.* provided a general strategy to coat a polymer shell *in situ* on a UCNC *via* UCNC-assisted photopolymerization using a 980 nm laser (Fig. 4e).[84] Two different UCNCs were utilized: $Na_{0.6}K_{0.4}YF_4$:Yb^{3+},Tm^{3+} for UV-light luminescence to excite a benzophenone/triethylamine (TEA) coinitiator system, and $NaYF_4$:Yb^{3+},Er^{3+} for visible-light luminescence to excite an Eosin Y/TEA system. After photopolymerization, UCNC core–polymer shell nanostructures were obtained, instead of the aggregates of the UCNC and polymer observed in Xiao and co-workers' study.[83] This method allowed the preparation of polymeric shells with various properties (*e.g.*, hydrophilic or hydrophobic, charged or neutral, containing various functional groups). Interestingly, a second polymeric shell such as a molecularly imprinted polymer (MIP) could also be synthesized on top of the UCNC core–polymer shell nanostructure after re-initiating the polymerization reaction in the presence of a molecular template (*e.g.*, trypsin) and MIP monomers.

Kocaarslan *et al.* performed free-radical polymerisation of poly (methyl methacrylate) (PMMA) using a tungsten-tellurite glass doped with Yb^{3+} and Tm^{3+} ions (UCG) as an internal light source.[85] The upconverted photons emitted from the UCG upon NIR light irradiation (975 nm) were used to excite a fluorescein photoinitiator (FL)/pentamethyldiethylene triamine coinitiator system. In addition, free radical-promoted cationic polymerization of oxirane, cyclohexene oxide, isobutyl vinyl ether and *N*-vinyl carbazole was also performed by first generating α-amino radicals from a FL dye/dimethyl aniline coinitiator system, subsequently oxidized by diphenyl iodonium hexafluorophosphate ($Ph_2I^+PF_6^-$) to form the initiating cations.

Reports on UCNC-assisted cycloaddition polymerization, free-radical polymerization, cationic polymerization, atom transfer radical polymerization, reversible addition–fragmentation chain transfer (RAFT) polymerization and reversible deactivation radical polymerization are found in ref. 86–92. It is important to

Open Access Article. Published on 13 2022. Downloaded on 28.01.2026 17:57:53.
This article is licensed under a Creative Commons Attribution-NonCommercial 3.0 Unported Licence.

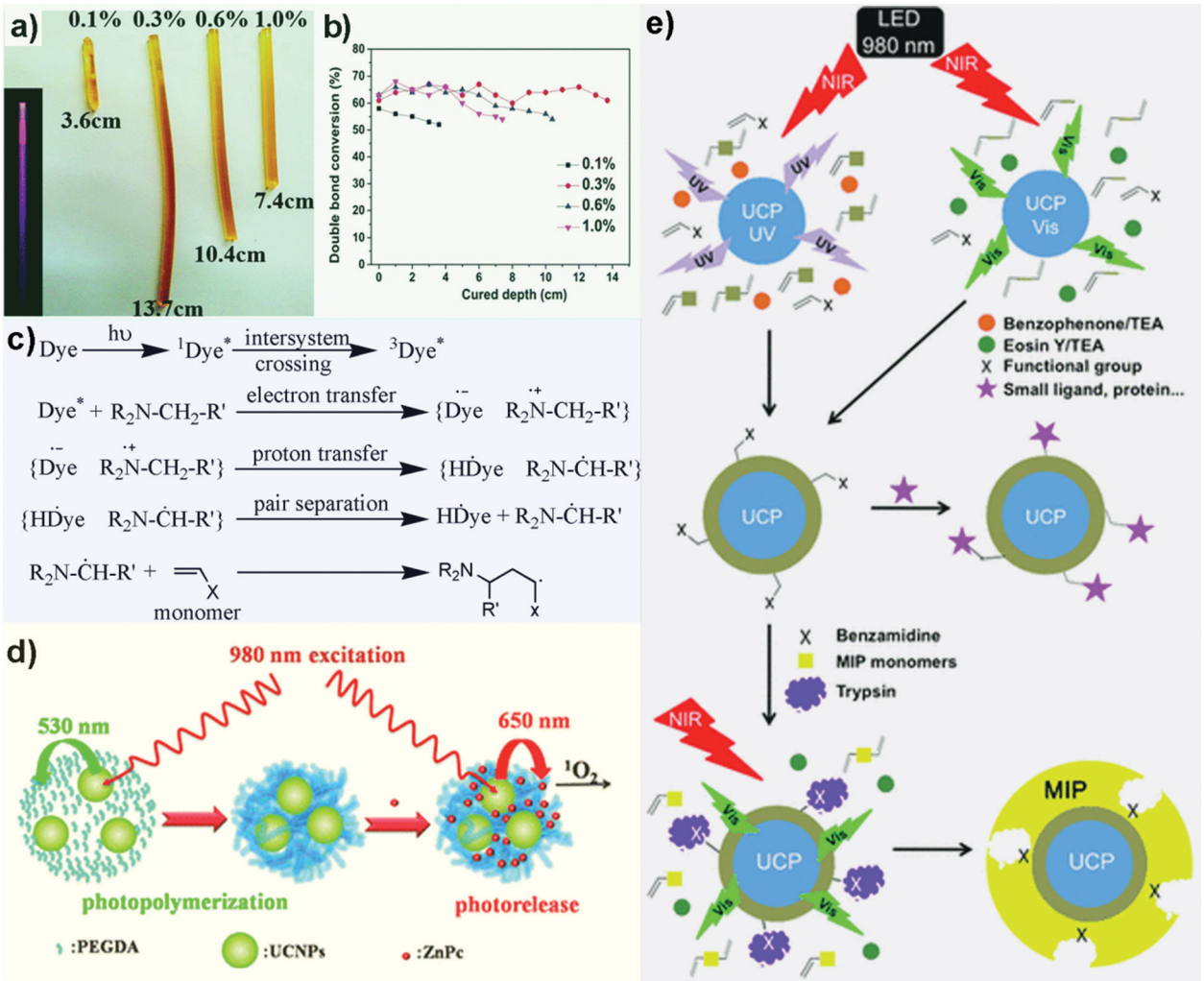

Fig. 4 (a) Curing depths obtained using different concentrations of $NaYF_4$:Yb^{3+},Tm^{3+} UCNC.[81] (b) Degree of monomer conversion at different curing depth.[81] Reprinted with permission from ref. 81. Copyright 2016, Royal Society of Chemistry. (c) Key steps to generate free radicals by the dye/coinitiator system.[82] Reprinted with permission from ref. 82. Copyright 2008, Wiley-VCH. (d) Schematic illustration of NIR light-activated photopolymerization of PEGDA hydrogels and NIR light-controlled release of singlet oxygen from ZnPc loaded into UCNP–PEGDA hybrid microspheres.[83] Reprinted with permission from ref. 83. Copyright 2013, Royal Society of Chemistry. (e) Schematic illustration of a generalized strategy to coat a polymer shell with different functional groups (X) on UCNC *via* UCNC-assisted photopolymerization and to further coat a molecularly imprinted polymer (MIP) layer in the presence of a molecular template (*e.g.*, trypsin) and MIP monomers.[84] Reprinted with permission from ref. 84. Copyright 2014, Wiley-VCH.

note that the success of photopolymerization is dependent on a few parameters including a high degree of spectral overlap between the emission of the UCNC ($E_{UCNC}(\lambda)$) and absorption of the photoinitiator/photosensitizer ($\varepsilon_{abs}(\lambda)$ is the molar extinction coefficient at wavelength λ):[93]

$$SOI(\lambda) = \int \varepsilon_{abs}(\lambda) \times E_{UCNC}(\lambda) d\lambda$$

and the initiation activity of the free radicals as discussed by Zou and co-workers.[94]

3. Lewis acid catalyst

Kang *et al.* have synthesized several hollow mesoporous ReF_3 (*e.g.*, LaF_3, NdF_3 and YF_3) nanocrystals in a mixture of tetrabutylammonium hexafluorophosphate ($N(Bu)_4PF_6$) and 1-octyl-3-methyl-imidazolium chloride (OmimCl) (Fig. 5).[95] It was reported that the Brunauer–Emmett–Teller (BET) surface area of the nanocrystals can be varied by tuning the ratio of the amounts of $N(Bu)_4PF_6$ to OmimCl. In addition, the as-prepared nanocrystals have loose structures with several crystal defects that act as LA catalytic sites. The authors tested the catalytic behaviour of their ReF_3 nanocrystals by performing the cyanosilylation of benzaldehyde using trimethylsilyl cyanide (TMSCN). At 50 °C and in a solventless environment, the cyanosilylation reaction was completed within 1 min, whereas a significantly lower conversion yield of the substrate was noted when a commercially purchased LaF_3, with a lower BET surface area, was used instead (*e.g.*, ~2.2% for benzaldehyde within 10 min). Clearly, the mesoporous ReF_3 nanocrystals exhibited higher

 This journal is © the Owner Societies 2022

Open Access Article. Published on 13 2022. Downloaded on 28.01.2026 17:57:53.
This article is licensed under a Creative Commons Attribution-NonCommercial 3.0 Unported Licence.

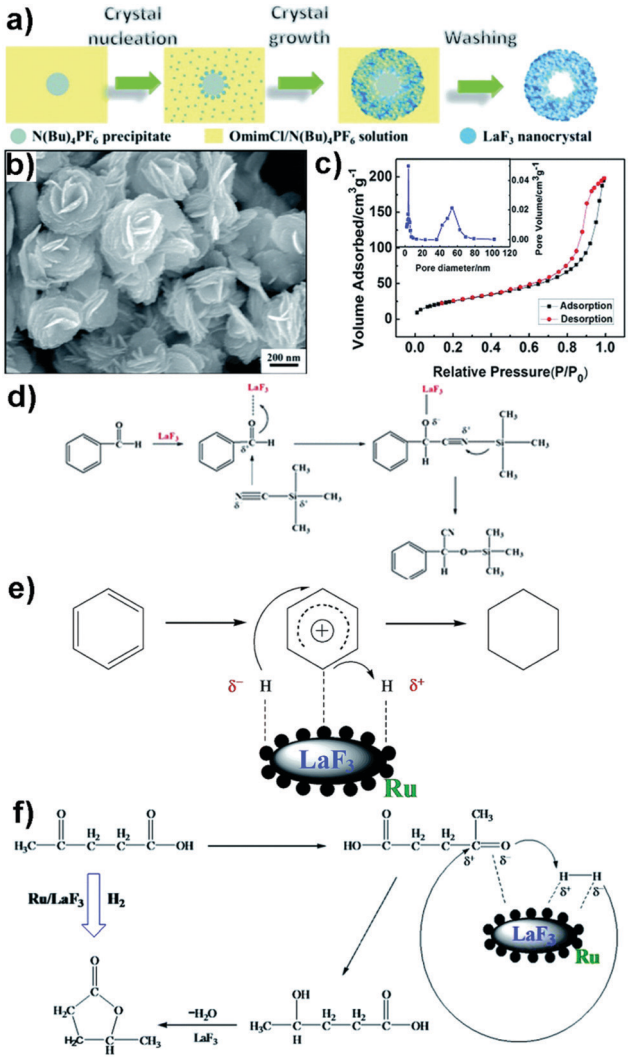

Fig. 5 (a) A scheme for the formation of hollow mesoporous ReF_3 (Re is La, Nd, or Y) nanocrystals. (b) SEM image of mesoporous LaF_3 nanocrystals. (c) Nitrogen adsorption and desorption isotherms of mesoporous LaF_3 nanocrystals shown in (b) (pore-size distribution is included in the inset). (d) Proposed reaction mechanism for the cyanosilylation reaction catalysed by LaF_3. (e) Proposed reaction mechanism for the benzene hydrogenation to cyclohexane using the co-catalyst Ru/LaF_3. (f) Proposed reaction mechanism for levulinic acid (LA) hydrogenation to γ-valerolactone using the co-catalyst Ru/LaF_3.[95] Reprinted with permission from ref. 95. Copyright 2015, Royal Society of Chemistry.

catalytic activity due to the presence of more LA sites created by crystal defects. A plausible three-step mechanism for the reaction was proposed (Fig. 5d); coordination of the O in the aldehyde to LA sites on the surface of the nanocrystals (step 1), attack of the CN group in TMSCN on the carbonyl group in the aldehyde (step 2), and isomerisation of the $Si(CH_3)_3$ group to form the product (step 3). The same authors also prepared a co-catalyst system by loading noble metals (*e.g.*, Ru nanoparticles) into mesoporous ReF_3 nanocrystals (*e.g.*, Ru/LaF_3 and Ru/NdF_3). The co-catalysts were then used for the efficient hydrogenation of benzene to cyclohexane (Fig. 5e) and levulinic acid to γ-valerolactone (Fig. 5f). In this case, the Ru metal activated H_2 whereas ReF_3 activated both the benzene ring and levulinic acid's carbonyl group.

Yu *et al.* synthesized hexagonal phase $NaScF_4$ and orthorhombic phase KSc_2F_7 nanocrystals *via* the co-thermolysis of $Na(CF_3COO)/K(CF_3COO)$ and $Sc(CF_3COO)_3$ in a binary oleic acid (OA)–oleylamine (OAm) solvent (Fig. 6a and b).[96] The nanocrystals were well-dispersed in polar solvents such as ethanol after thermal treatment at 500 °C in Ar/H_2 for 1 h to remove the coordinating ligands (Fig. 6c). The cyanosilylation reaction of electron-rich and electron-poor aromatic aldehydes by TMSCN was performed in the presence of either $NaScF_4$ or KSc_2F_7 nanocrystals to afford excellent product yields under standard conditions (catalyst: 5 mol%; temperature: 25 °C; time: 24 h). In addition, the recycled scandium-based nanocatalysts showed excellent catalytic behaviour even after 10 repeated runs (Fig. 6d).

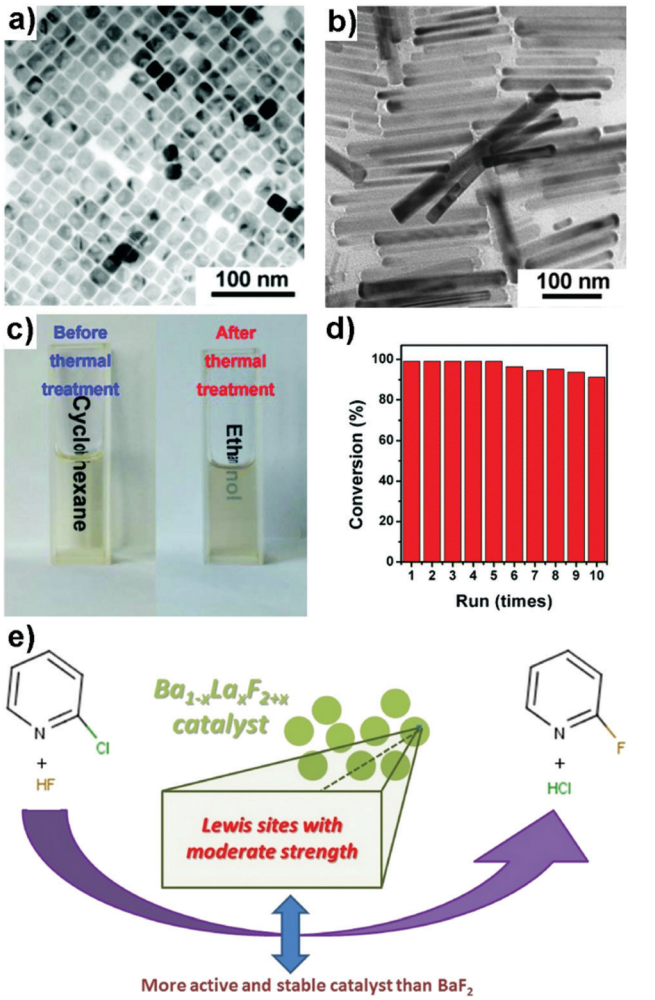

Fig. 6 TEM images of (a) $NaScF_4$ and (b) KSc_2F_7 nanocrystals. (c) Photograph of $NaScF_4$ nanocrystal solutions before and after thermal treatment at 500 °C under Ar/H_2. (d) Reusability test of $NaScF_4$ nanocrystals for 10 cycles in the cyanosilylation reaction.[96] Reprinted with permission from ref. 96. Copyright 2017, Royal Society of Chemistry. (e) A scheme for the gas phase fluorination of 2-chloropyridine by HF using $Ba_{1-x}La_xF_{2+x}$.[97] Reprinted with permission from ref. 97. Copyright 2017, Elsevier.

Open Access Article. Published on 13 2022. Downloaded on 28.01.2026 17:57:53.
This article is licensed under a Creative Commons Attribution-NonCommercial 3.0 Unported Licence.

Astruc *et al.* reported the synthesis of $Ba_{1-x}La_xF_{2+x}$ fluoride nanomaterials (*e.g.*, $Ba_{0.5}La_{0.5}F_{2.5}$ and $Ba_{0.1}La_{0.9}F_{2.9}$) for the gas phase fluorination of 2-chloropyridine by HF (Fig. 6e).[97] The introduction of LaF_3 played several important roles in enhancing the catalytic performance of the bimetallic fluoride: (a) LaF_3 significantly increased the stability of BaF_2 in a wet environment by reducing the sintering of BaF_2 in water, (b) LaF_3 resulted in a higher surface area and more LA catalytic sites, and (c) LaF_3 prevented the chlorination of the BaF_2 catalyst by HCl. In a separate study by Li and co-workers, YF_3 nanoflowers were demonstrated to be an efficient catalyst for the electrochemical nitrogen reduction reaction under ambient conditions.[98] The electrocatalyst elongated the N≡N bond and activated it to promote the adsorption of H atoms in various hydrogenation steps to form NH_3(g).

4. Photothermal materials

4.1. Light-to-heat conversion mechanism

The most commonly used sensitizer in Re fluoride nanocrystals for photothermal applications is Nd^{3+} which is excited from its $^4I_{9/2}$ ground state to an excited state ($^4F_{5/2}$) by ~800 nm light.[69,70,99–101] At this wavelength, the light penetrates deep into biological tissues, and overheating is avoided due to the low absorption of light by water (*i.e.*, absorption coefficients of water at 808 nm and 980 nm are 0.02 cm^{-1} and 0.48 cm^{-1}, respectively).[102,103] In a matrix sparsely doped with Nd^{3+} (*e.g.*, $NaYF_4$:Nd^{3+}), an excited ion relaxes from the $^4F_{5/2}$ state to $^4F_{3/2}$ state before undergoing radiative relaxation to the $^4I_{15/2}$, $^4I_{13/2}$, $^4I_{11/2}$ and $^4I_{9/2}$ states. Subsequently, non-radiative relaxation from either of the $^4I_{x/2}$ (x = 15, 13 and 11) state to the $^4I_{9/2}$ ground state releases heat (Fig. 7a).[70] When the concentration of the dopant is increased (*e.g.*, $NaNdF_4$, NdF_3), the distance between Nd^{3+} ions is reduced and inter-ionic interactions are enhanced. In this case, an excited Nd^{3+} ion in close proximity to a relaxed Nd^{3+} ion can undergo efficient cross-relaxation, whereby the excited ion de-excites from the $^4F_{3/2}$ state to the $^4I_{15/2}$ state (energy gap = 5749 cm^{-1}), and the partner ion in the ground state is promoted from the $^4I_{9/2}$ state to the $^4I_{15/2}$ state (energy gap = 5851 cm^{-1}).[99] Both ions in the $^4I_{15/2}$ state subsequently return to the $^4I_{9/2}$ ground state *via* a non-radiative relaxation process that generates heat. Another plausible mechanism to understand the photothermal effect is energy migration between Nd^{3+} ions followed by energy trapping by non-radiative centres (*e.g.*, surface ligands, defect sites and surrounding solvent) that release heat upon their relaxation.

Tikhomirov *et al.* have also demonstrated the photothermal effect in a matrix containing both the Yb^{3+} sensitizer and Er^{3+} activator ions (*i.e.*, $Re_{10}Pb_{25}F_{65}$ nanoparticles where Re: Yb^{3+}–Er^{3+}).[104] Energy transfer from the photoexcited Yb^{3+} to Er^{3+} gave rise to the population of the $^2H_{11/2}$, $^4S_{3/2}$ and $^4F_{9/2}$ states of Er^{3+} which radiatively emit upconverted energy photons (see discussion in Section 2). At the same time, due to a non-resonant energy transfer process, a mismatch in energy occurred and the excess energy was released as phonon emission (depicted by wavy lines in Fig. 7b) which increased the surrounding temperature. In a separate study, Zhao *et al.* have shown that non-radiative relaxation of Tm^{3+} ions in CeO_2:Yb^{3+},Tm^{3+} nanospheres, after energy transfer from photoexcited Yb^{3+}, did not significantly alter the matrix temperature, and the observed photothermal effect was instead attributed to energy migration between Yb^{3+} ions before energy trapping by non-radiative surface quenchers.[105]

4.2. Light-to-heat conversion efficiency determination

The temperature of PTM in photothermal catalysis can be measured using various experimental approaches including non-luminescence methods (*e.g.*, scanning thermal microscopy and scanning transmission electron microscopy) and luminescence methods (*e.g.*, IR thermography, thermoreflectance, optical interferometry and luminescent nanothermometers).[73] Among these approaches, IR thermography is the most commonly used to measure the temperature by detecting radiation (*i.e.*, heat) from the targeted PTM. The light-to-heat conversion efficiency (η) of PTM in a solution is determined using the following equation:[68,106–108]

$$\eta = \frac{hS(T_{max} - T_{surr}) - Q_{dis}}{I_0(1 - 10^{-A_{exc}})}$$

where h is the heat transfer coefficient, S is the surface area of the container, T_{max} is the equilibrium temperature, T_{surr} is the ambient surrounding temperature, Q_{dis} is the energy input due to the solvent and container, I_0 is the incident laser power and A_{exc} is the absorbance at the excitation wavelength. Q_{dis} is obtained by measuring the temperature change of the solvent ΔT and is calculated using the following equation:

$$Q_{dis} = \frac{10^3 \times m \times C \times \Delta T}{t}$$

where m is the mass of the solvent used, C is the heat capacity of the solvent used, ΔT is the obtained increase in the temperature and t is the laser exposure time. In order to obtain hS, a dimensionless driving force temperature θ is defined:

$$\theta = \frac{T - T_{surr}}{T_{max} - T_{surr}}$$

such that when the laser source is turned off, the cooling process that follows can be described by:

$$t = -\tau_s \ln \theta$$

where T is the temperature of the solution at time t. hS is thus obtained from $hS = (mC)/\tau_s$. From the cooling curve, τ_s is obtained by linearly fitting the plot of the cooling time t *versus* the term $-\ln \theta$.

4.3. Parameters affecting photothermal efficiency

In this section, we briefly discuss the various parameters that affect the photothermal performance of the Re fluoride nanocrystals. Bednarkiewicz *et al.* have synthesized α-$NaYF_4$ nanocrystals doped with various concentrations of Nd^{3+} using a thermal deposition method.[99] It was noted that when the

Open Access Article. Published on 13 2022. Downloaded on 28.01.2026 17:57:53.
This article is licensed under a Creative Commons Attribution-NonCommercial 3.0 Unported Licence.

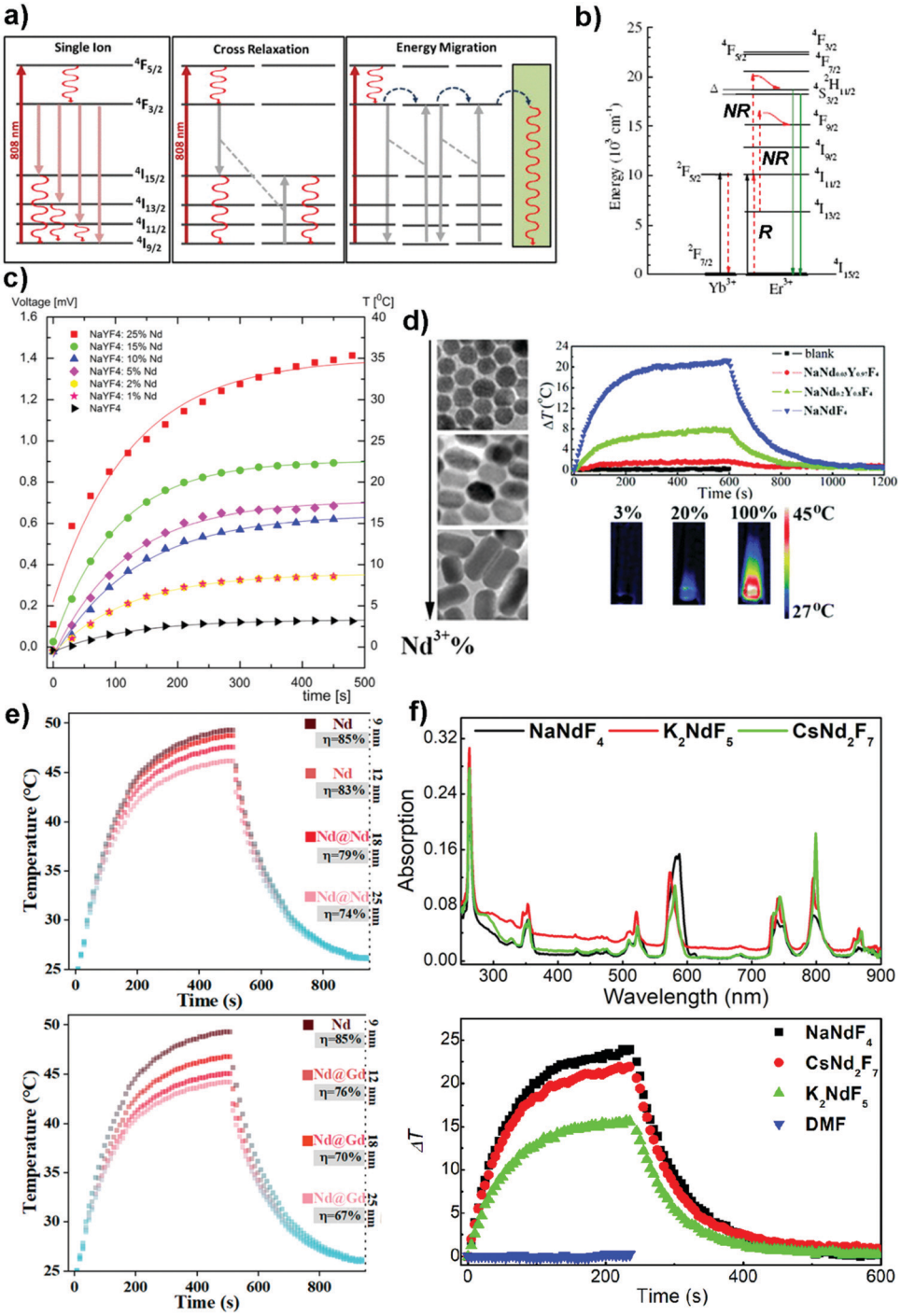

Fig. 7 (a) Simplified energy levels of Nd^{3+} ions and photophysical processes that lead to photothermal effect after 808 nm light irradiation.[70] Reprinted with permission from ref. 70. Copyright 2014, AIP Publishing LLC. (b) Simplified energy levels of Yb^{3+} and Er^{3+} ions, and photophysical processes after 975 nm light irradiation.[104] Reprinted with permission from ref. 104. Copyright 2009, The Optical Society. (c) Temperature change profiles of a cyclohexane solution of cubic phase $NaYF_4$ nanocrystals doped with Nd^{3+} (1–25%) excited using an 808 nm laser.[99] Reprinted with permission from ref. 99. Copyright 2011, Elsevier. (d) TEM images of $NaYF_4$ nanocrystals doped with different amounts of Nd^{3+} to illustrate the effects of dopant concentration on the morphology and photothermal performance of $NaYF_4$:Nd^{3+} (3%, 20% and 100%) nanocrystals.[68] Reprinted with permission from ref. 68. Copyright 2019, Royal Society of Chemistry. (e) Effects of the thickness of $NaNdF_4$ (upper panel) and $NaGdF_4$ (lower panel) shells on the temperature change.[110] Reprinted with permission from ref. 110. Copyright 2020, American Chemical Society. (f) Absorption spectra of $NaNdF_4$, K_2NdF_5 and $CsNd_2F_7$ nanocrystals (upper panel) and their corresponding temperature change profile (lower panel) obtained after being excited using an 808 nm laser.[107] Reprinted with permission from ref. 107. Copyright 2021, American Chemical Society.

Open Access Article. Published on 13 2022. Downloaded on 28.01.2026 17:57:53.
This article is licensed under a Creative Commons Attribution-NonCommercial 3.0 Unported Licence.

amount of doped Nd^{3+} is <25%, the size and morphology of the nanocrystals remain relatively similar. However, the maximum temperature change increased linearly with dopant concentration; a consequence of a stronger cross-relaxation interaction between the Nd^{3+} ions (Fig. 7c).

Wu *et al.* demonstrated that the luminescence intensity and lifetime of $NaNd_xY_{1-x}F_4$ nanocrystals gradually decreased with an increase in the concentration of Nd^{3+} whereas the light-to-heat conversion efficiency η increased (*e.g.*, $\eta(NaNd_{0.03}Y_{0.97}F_4) \sim 0.066 < \eta(NaNd_{0.2}Y_{0.8}F_4) \sim 0.15 < \eta(NaNdF_4) \sim 0.213$).[68] The inverse relationship between light-to-heat conversion efficiency and luminescence intensity was also noted when the host matrix was changed to $LiYF_4$. This made the nanocrystals doped with different concentration of Nd^{3+} good candidates for anti-counterfeiting labels with opposite displays (Fig. 7d).

The effects of the nanocrystal size and laser excitation wavelength on the light-to-heat conversion efficiency of β-$NaNdF_4$ were investigated by Ding and co-workers.[109] $NaNdF_4$ nanocrystals of various sizes (*i.e.*, 4.7, 5.9, 12.8, and 15.6 nm) were first prepared by controlling the Ostwald ripening time. It was reported that nanocrystals exhibited better photothermal properties when exposed to an 808 nm laser as compared to a 793 nm laser. Furthermore, the nanocrystal with a diameter of ~12.8 nm displayed the best photothermal performance, however, an explanation for this observation was not provided.

Li *et al.* have synthesized β-$NaNdF_4$ nanocrystals of different sizes (*i.e.*, diameter d = 9, 12, 18 and 25 nm) using a hot injection method.[110] The light-to-heat conversion efficiency (η) of 85% measured for the $NaNdF_4$ nanocrystals with d = 9 nm was reduced to 74% when d was increased to 25 nm. Depositing an 8 nm thick $NaGdF_4$ shell onto the $NaNdF_4$ core only reduced η by 18% (Fig. 7e). The authors rationalized the above data using the concept of surface quenching suppression, however, they concluded that the main contribution to the photothermal effect came from cross-relaxation interaction between neighbouring Nd^{3+} ions. In addition, the authors reported that the equilibrium temperature reached increased with an increase in the laser power.

Very recently, we have reported a facile co-precipitation method of synthesizing orthorhombic phase $CsNd_2F_7$ and hexagonal phase K_2NdF_5 nanocrystals that avoids harsh conditions (*e.g.*, high temperatures and long reaction times in hydrothermal synthesis) (Fig. 7f).[107] The as-prepared nanocrystals were stable in basic solutions (*e.g.*, 1-octadecene/OAm/OA with OAm:OA molar ratio ~1.6) but decomposed to hexagonal phase NdF_3 or orthorhombic phase $KNdF_4$ in acidic solutions (*e.g.*, 1-octadecene/OA) at a high reaction temperature (*e.g.*, ~300 °C). In addition, the nanocrystals exhibited good photothermal performance (*i.e.*, $\eta(CsNd_2F_7) \sim 26.6 \pm 3.4\%$ and $\eta(K_2NdF_5) \sim 16.2 \pm 1.5\%$). The absorption spectra of the tetra-, penta- and heptafluoride nanocrystals did not change significantly despite differences in their size, morphology, and crystalline phase. This is different from other PTMs (*e.g.*, gold and silver) whose absorption peaks are strongly dependent on the size and morphology of the nanocrystals.

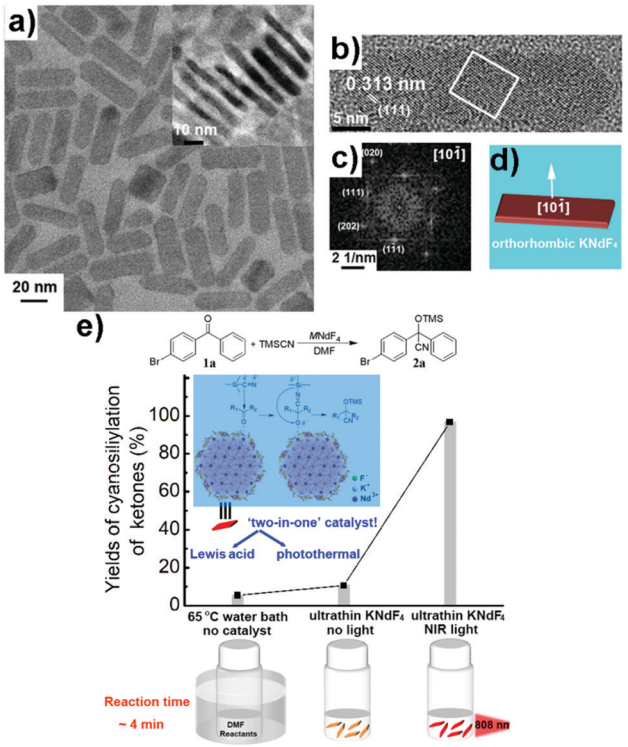

Fig. 8 (a) TEM image of orthorhombic $KNdF_4$ nanoplates (inset shows the TEM image of single nanoplates standing on their edge). (b) HRTEM image of a single nanoplate with a length of 34.1 nm and a width of 10.2 nm. (c) the FFT pattern with [10$\bar{1}$] zone axis for the white-boxed area in (b). (d) Scheme of nanoplate growth. (e) A scheme to show the synergistic effects from NIR light activated $KNdF_4$ nanoplates on the product yields of the cyanosilylation of 4-bromobenzophenone by TMSCN.[108] Reprinted with permission from ref. 108. Copyright 2020, Wiley-VCH.

4.4. Applications of the photothermal effect in catalytic reactions

Recently, we prepared ultrathin (*i.e*, 3–4 unit cell layers) $KNdF_4$ nanoplates as a synergistic 'two-in-one' nanocatalyst, combining both Lewis acid and photothermal effect, for the cyanosilylation of ketones with TMSCN (Fig. 8).[108] Near quantitative product yields were observed within a short reaction time (*e.g.*, 4 min) when the reaction mixture containing the $KNdF_4$ nanoplates (~4.8 mol%) was irradiated with an 808 nm laser. The surface Nd^{3+} ions endowed LA with catalytic activity whereas the photothermally generated heat improved the reaction rate. Thermal stability is an important requirement for PTM. Even though Au nanostructures have excellent photothermal performances, changes in their size and morphology are usually seen when exposed to light irradiation.[57,58] Compared to Au nanostructures, the $KNdF_4$ nanoplates are thermally stable. Their morphology remained relatively intact even after five cycles of cyanosilylation reactions conducted at a reaction temperature of 52 °C.

5. Conclusion and perspective

In summary, we have introduced the applications of rare-earth fluoride nanocrystals in facilitating organic synthetic and

 This journal is © the Owner Societies 2022

Open Access Article. Published on 13 2022. Downloaded on 28.01.2026 17:57:53.
This article is licensed under a Creative Commons Attribution-NonCommercial 3.0 Unported Licence.

polymerization reactions using either one or a combination of their unique features, namely as a Lewis acid catalyst, upconversion luminescence nanolamp or photothermal nanoheater. This research is still in its early stages of development and growth, and several challenges exist that warrant further investigation as discussed below.

5.1. Enhancing upconversion luminescence and using solar energy

Since IR light accounts for more than half of the solar spectrum (*i.e.*, 51%, 47% and 2% of solar light is made up of IR, visible and UV light, respectively), it would be ideal if solar energy becomes a viable excitation source. By focusing sunlight onto $BaCl_2$:Ho^{3+} that absorbed maximally at 900, 1157 and 1610 nm using an optical lens, Jia *et al.* successfully measured its upconversion luminescence.[111] To further improve the utilization of solar energy, it is worthwhile to explore the use of effective methods to harvest both visible and IR light of the solar spectrum as an excitation source (*e.g.*, by using luminescent solar concentrators).[8,112]

One of the limitations of lanthanide-based UCNCs is the low conversion yield of NIR to UV/visible light (<1%). To improve the intensity of upconversion luminescence without the need for increasing laser intensity or concentration of UCNC, several strategies including plasmon-assisted upconversion, core–shell structure design, dye-sensitized UCNC, and host lattice distortion have been proposed.[1,9–11,23,103,113] This is particularly useful when overheating, due to the photothermal effect of lanthanide-based UCNC or absorption of excitation light by the solvent, is not desired in a photochemical/photopolymerization reaction. In this case, it is advantageous to be able to produce strong upconversion emission using as low an excitation intensity as possible. The ultimate aim is to employ UCNCs as an efficient NIR-light activated nanolamp to drive scaled-up reactions in industries, and hence the quest to easily and economically prepare brighter UCNCs is both pertinent and necessary.

5.2. Generating more Lewis acid catalytic sites

Since functional groups (*e.g.*, $-COO^-$, $-NH_2$ and –SH) can coordinate with lanthanide ions on the surface of the nanocrystals, capping ligands (*e.g.*, oleate and oleylamine) are usually used in the synthesis to stabilize the (alkaline) Re fluoride nanocrystals.[17,68,107,108,114,115] In order to generate more Lewis acid sites, a straightforward approach is to remove the protecting ligands using different strategies such as ligand exchange and thermal treatment.[96,108,116] LA sites can also be generated from crystal defects which are usually introduced during the synthesis of nanocrystals. Defects found in nanocrystals with poor crystalline quality and large surface-to-volume ratio can be prepared by tuning the synthesis parameters such as using lower reaction temperatures and shorter reaction times, and introducing extra dopant ions.[117]

5.3. Improving photothermal performance

The following properties are often considered when designing a functional PTM: (i) strong absorption of light across a wide range of the solar spectrum, (ii) efficient light-to-heat conversion efficiency and (iii) high thermal stability. Similar methods introduced in Section 5.1 can be applied to enhance the absorption of light. On the other hand, options to improve the photothermal effect of lanthanide-based nanomaterials are scarce. By coating $NaNdF_4$ with Prussian Blue (PB), Yu *et al.* observed a remarkable light-to-heat conversion efficiency of 60.8%.[118] The authors attributed the better performance of the $NaNdF_4$@PB core/shell nanocomplex to a new cross-relaxation process between excited Nd^{3+} and excited PB that populated more of the $^4F_{3/2}$ state of the lanthanide needed to generate heat. The same technique was also used to enhance the light-to-heat conversion efficiency of a $NaErF_4$@$NaYF_4$@$NaNdF_4$ core/shell/shell nanocrystal.[119] Other methods that do not involve the use of dye molecules that may suffer from thermal- and photodegradation are attractive and deserve further investigation.

Re fluoride nanomaterials are non-conducting as the 4f electrons of lanthanides are well shielded by their filled $5s^25p^6$ orbitals; charge carriers generated from photoexcitation do not participate in catalytic reactions.[7,11,13,14,120] Instead, these nanomaterials aid in increasing the surrounding temperature and enhancing reaction rates. An area that is currently lacking is the exploitation of Re fluoride nanocrystals as PTMs in conjunction with photoredox catalysts (*e.g.*, MOFs, organometallic complexes, and organic dyes) to drive photocatalytic reactions.

The ratio of the upconversion luminescence intensity of the thermally coupled $^2H_{11/2} \rightarrow {}^4I_{15/2}$ transition (520 nm) and $^4S_{3/2} \rightarrow {}^4I_{15/2}$ transition (540 nm) of Er^{3+} in a tetrafluoride matrix co-doped with Yb^{3+} and Er^{3+} has been shown to be a convenient readout in ratiometric thermometry.[121,122] By constructing a nanocomposite containing a lanthanide-based nanocrystal in a covalent organic framework that was crafted with Cu ions, Krishnaraj *et al.* managed to perform simultaneous Cu-catalyzed reaction of indole, aldehyde and malononitrile to yield 2-((1*H*-indol-3-yl)(phenyl)methyl)malononitrile, and nanothermometry to track the local temperature of the reaction.[123] It would therefore be useful to explore the possibility of generating heat from lanthanide-based nanoheaters in catalytic reactions while concurrently measuring the internal temperature of the reaction mixture using the same PTM.

When employing a combination of the upconversion emission and photothermal effect of lanthanide-based nanomaterials, their inverse relationship should be taken into account. To optimize the usage of each property in a single system, the structural design of the nanocrystal by confining each function to a specific area (*e.g.*, upconversion luminescence to the core and photothermal to the shell) may address this issue in future applications.

5.4. Toxicity and environmental impact

Studies on the toxicity of lanthanide-based upconversion nanomaterials have generally shown that they have low toxicity.[124,125] For example, ligand-free α-$NaYF_4$:Yb^{3+},Tm^{3+} and ligand-free core–shell α-$NaYF_4$:Yb^{3+},Er^{3+}@$NaLuF_4$ have no side effects

Open Access Article. Published on 13 2022. Downloaded on 28.01.2026 17:57:53.
This article is licensed under a Creative Commons Attribution-NonCommercial 3.0 Unported Licence.

when accumulated in human pancreatic cancer cells (Panc 1) and *Caenorhabditis elegans* worms, respectively.[126,127] Caution should still be exercised to ensure that potentially harmful lanthanide ions and ligands are not leached into the solution. Another area of concern is the lack of a standard protocol to test and assess the toxicity of the various lanthanide-based nanomaterials.[128] A systematic comparison between nanostructures is best made when a uniform set of factors such as size, morphology, crystalline phase, types of surface ligands, chemical compositions, *etc.* is considered.

The impact of lanthanide-based nanomaterials on the environment and ecosystem has received less attention. A study previously reported that plants can uptake water soluble $NaYF_4$:Yb^{3+},Er^{3+} upconversion nanoparticles through the roots with minimal detrimental effects.[129] In fact, the growth of mung bean plants was demonstrated to improve due to better water absorption caused by $NaYF_4$:Yb^{3+},Er^{3+}@CDs nanocomposites, where CDs are carbon dots.[130] Future studies on the positive and negative impact of the interaction of lanthanide-based nanomaterials with soil, water and air are warranted.

Author contributions

X. W. and E. K. L. Y. proposed the topic of this review, interpreted the relevant literature and co-wrote the manuscript.

Conflicts of interest

There are no conflicts to declare.

Acknowledgements

We acknowledge financial support from the Singapore Ministry of Education MoE Tier 1 grant (RG89/20).

References

1 S. Han, R. Deng, X. Xie and X. Liu, Enhancing luminescence in lanthanide-doped upconversion nanoparticles, *Angew. Chem., Int. Ed.*, 2014, **53**, 2.
2 S. P. Tiwari, S. K. Maurya, R. S. Yadav, A. Kumar, V. Kumar, M.-F. Joubert and H. C. Swart, Future prospects of fluoride based upconversion nanoparticles for emerging applications in biomedical and energy harvesting, *J. Vac. Sci. Technol., B*, 2018, **36**, 060801.
3 R. Wang and F. Zhang, in *Near-infrared Nanomaterials: Preparation, Bioimaging and Therapy Applications*, ed. F. Zhang, Royal Society of Chemistry, Cambridge, UK, 2016, ch. 1, pp. 1–39.
4 Y.-F. Wang, G.-Y. Liu, L.-D. Sun, J.-W. Xiao, J.-C. Zhou and C.-H. Yan, Nd^{3+}-sensitized upconversion nanophosphors: efficient in vivo bioimaging probes with minimized heating effect, *ACS Nano*, 2013, **7**, 7200.
5 M. Tan and G. Chen, in *Near Infrared-Emitting Nanoparticles for Biomedical Applications*, ed. A. Benayas, E. Hemmer, G. Hong and D. Jaque, Springer Nature, Switzerland AG, 2020, ch. 4, pp. 63–81.
6 W. Yang, X. Li, D. Chi, H. Zhang and X. Liu, Lanthanide-doped upconversion materials: emerging applications for photovoltaics and photocatalysis, *Nanotechnology*, 2014, **25**, 482001.
7 K. Zheng, K. Y. Loh, Y. Wang, Q. Chen, J. Fan, T. Jung, S. H. Nam, Y. D. Suh and X. Liu, Recent advances in upconversion nanocrystals: Expanding the kaleidoscopic toolbox for emerging applications, *Nano Today*, 2019, **29**, 100797.
8 B. S. Richards, D. Hudry, D. Busko, A. Turshatov and I. A. Howard, Photon upconversion for photovoltaics and photocatalysis: a critical review, *Chem. Rev.*, 2021, **121**, 9165.
9 S. Gai, C. Li, P. Yang and J. Lin, Recent progress in rare earth micro/nanocrystals: soft chemical synthesis, luminescent properties, and biomedical applications, *Chem. Rev.*, 2014, **114**, 2343.
10 X. Zhu, J. Zhang, J. Liu. and Y. Zhang, Recent progress of rare-earth doped upconversion nanoparticles: synthesis, optimization, and applications, *Adv. Sci.*, 2019, **6**, 1901358.
11 X. Li, F. Zhang and D. Zhao, Lab on upconversion nanoparticles: optical properties and applications engineering via designed nanostructure, *Chem. Soc. Rev.*, 2015, **44**, 1346.
12 G. Chen, H. Qiu, P. N. Prasad and X. Chen, Upconversion nanoparticles: design, nanochemistry, and applications in theranostics, *Chem. Rev.*, 2014, **114**, 5161.
13 A. Kar and A. Patra, Impacts of core–shell structures on properties of lanthanide-based nanocrystals: crystal phase, lattice strain, downconversion, upconversion and energy transfer, *Nanoscale*, 2012, **4**, 3608.
14 R. K. Sharma, A.-V. Mudring and P. Ghosh, Recent trends in binary and ternary rare-earth fluoride nanophosphors: How structural and physical properties influence optical behaviour, *J. Lumin.*, 2017, **189**, 44.
15 J. S. Lee, D. H. Nam, S. K. Kuk and C. B. Park, Near-infrared-light-driven artificial photosynthesis by nano-biocatalytic assemblies, *Chem. – Eur. J.*, 2014, **20**, 3584.
16 M. Freitag, N. Möller, A. Rühling, C. A. Strassert, B. J. Ravoo and F. Glorius, Photocatalysis in the dark: near-infrared light driven photoredox catalysis by an upconversion nanoparticle/photocatalyst system, *ChemPhotoChem*, 2018, **2**, 1.
17 Q. Du, X. Wu, W. Bi, B. G. Xing and E. K.-L. Yeow, Increasing antibiotic activity by rapid bioorthogonal conjugation of drug to resistant bacteria using an upconverted light-activated photocatalyst, *J. Mater. Chem. B*, 2021, **9**, 3136.
18 Y. Wu, J. Zheng, D. Xing and T. Zhang, Near-infrared light controlled fluorogenic labeling of glycoengineered sialic acids in vivo with upconverting photoclick nanoprobe, *Nanoscale*, 2020, **12**, 10361.
19 S. Wu, J. P. Blinco and C. Barner-Kowollik, Near-infrared photoinduced reactions assisted by upconverting nanoparticles, *Chem. – Eur. J.*, 2017, **23**, 8325.

Open Access Article. Published on 13 2022. Downloaded on 28.01.2026 17:57:53.
This article is licensed under a Creative Commons Attribution-NonCommercial 3.0 Unported Licence.

20 Z. Wang, D. C. Thang, Q. Han, X. Zhao, X. Xie, Z. Wang, J. Lin and B. G. Xing, Near-infrared photocontrolled therapeutic release via upconversion nanocomposites, *J. Controlled Release*, 2020, **324**, 104.
21 S. Wu and H.-J. Butt, Near-infrared photochemistry at interfaces based on upconverting nanoparticles, *Phys. Chem. Chem. Phys.*, 2017, **19**, 23585.
22 Y. Tang and G. Wang, NIR light-responsive nanocarriers for controlled release, *J. Photochem. Photobiol., C*, 2021, **47**, 100420.
23 Y. Wu, S. Y. Chan, J. Xu and X. Liu, Multiphoton upconversion materials for photocatalysis and environmental remediation, *Chem. – Asian J.*, 2021, **16**, 2596.
24 Z. Zhang, Y. Liu, Y. Fang, B. Cao, J. Huang and K. Liu, Bin Dong, Near-infrared-plasmonic energy upconversion in a nonmetallic heterostructure for efficient H_2 evolution from ammonia borane, *Adv. Sci.*, 2018, **5**, 1800748.
25 M.-Q. Yang, M. Gao, M. Hong and G. W. Ho, Visible-to-NIR photon harvesting: progressive engineering of catalysts for solar-powered environmental purification and fuel production, *Adv. Mater.*, 2018, **30**, 1802894.
26 A. A. Ansari and M. Sillanpää, Advanced in upconversion nanoparticles based NIR-driven photocatalysts, *Renewable Sustainable Energy Rev.*, 2021, **151**, 111631.
27 B. Li, Y. Hu, Z. Shen, Z. Ji, L. Yao, S. Zhang, Y. Zou, D. Tang, Y. Qing, S. Wang, G. Zhao and X. Wang, Photocatalysis driven by near-infrared light: materials design and engineering for environmentally friendly photoreactions, *ACS ES&T Eng.*, 2021, **1**, 947.
28 M. Zhong, Z. Wang, D. Dai, B. Yang, S. Zuo, C. Yao, F. Wu and X. Li, Upconversion hollow nanospheres CeF_3 co-doped with Yb^{3+} and Tm^{3+} for photocatalytic nitrogen fixation, *J. Rare Earths*, 2022, **40**, 586.
29 C. He, X. Li, X. Chen, S. Ma, X. Yan, Y. Zhang, S. Zuo and C. Yao, Palygorskite supported rare earth fluoride for photocatalytic nitrogen fixation under full spectrum, *Appl. Clay Sci.*, 2020, **184**, 105398.
30 S. Zuo, H. Zhang, X. Li, C. Han, C. Yao and C. Ni, Dual active sites boosting photocatalytic nitrogen fixation over upconversion mineral nanocomposites under the full spectrum, *ACS Sustainable Chem. Eng.*, 2022, **10**, 1440.
31 W. Fan, H. Bai and W. Shi, Semiconductors with NIR driven upconversion performance for photocatalysis and photoelectrochemical water splitting, *CrystEngComm*, 2014, **16**, 3059.
32 C. K. Chen, H. M. Chen, C.-J. Chen and R.-S. Liu, Plasmon-enhanced near-infrared-active materials in photoelectrochemical water splitting, *Chem. Commun.*, 2013, **49**, 7917.
33 K. Feng, Z. Cai, D. Huang, L. Li, K. Wang, Y. Li, C. Wang, J. Song, L. Zhao, W. Wei and F. Jiang, Near-infrared-driven water splitting for hydrogen evolution using a Cu_2ZnSnS_4-based photocathode by the application of upconversion nanoparticles, *Sustain, Energy Fuels*, 2020, **4**, 2669.
34 M. Zhang, Y. Lin, T. J. Mullen, W.-F. Lin, L.-D. Sun, C.-H. Yan, T. E. Patten, D. Wang and G.-Y. Liu, Improving hematite's solar water splitting efficiency by incorporating rare-earth upconversion nanomaterials, *J. Phys. Chem. Lett.*, 2012, **3**, 3188.
35 S. Reischauer and B. Pieber, Emerging concepts in photocatalytic organic synthesis, *iScience*, 2021, **24**, 102209.
36 F. Strieth-Kalthoff, M. J. James, M. Teders, L. Pitzer and F. Glorius, Energy transfer catalysis mediated by visible light: principles, applications, directions, *Chem. Soc. Rev.*, 2018, **47**, 7190.
37 M. H. Shaw, J. Twilton and D. W.-C. MacMillan, Photoredox catalysis in organic chemistry, *J. Org. Chem.*, 2016, **81**, 6898.
38 G. E.-M. Crisenza and P. Melchiorre, Chemistry glows green with photoredox catalysis, *Nat. Commun.*, 2020, **11**, 803.
39 H. Hayashi, B. Wang, X. Y. Wu, S. J. Teo, A. Kaga, K. Watanabe, R. Takita, E. K.-L. Yeow and S. Chiba, Biaryl cross-coupling enabled by photo-induced electron transfer, *Adv. Synth. Catal.*, 2020, **362**, 2223.
40 Y. Z. Tan, X. Y. Wu, T. N. Do, H. L. Nguyen, H.-S. Tan, S. Chiba and E. K.-L. Yeow, Electron transfer quenching of Rhodamine 6G by N-methylpyrrole is an unproductive process in the photocatalytic heterobiaryl cross-coupling reaction, *J. Phys. Chem. B*, 2021, **125**, 8550.
41 A. Mavridi-Printezi, A. Menichetti, M. Guernelli and M. Montalti, Extending photocatalysis to the visible and NIR: the molecular strategy, *Nanoscale*, 2021, **13**, 9147.
42 B. D. Ravetz, A. B. Pun, E. M. Churchill, D. N. Congreve, T. Rovis and L. M. Campos, Photoredox catalysis using infrared light via triplet fusion upconversion, *Nature*, 2019, **565**, 343.
43 F. Wang, C. Li, H. Chen, R. Jiang, L.-D. Sun, Q. Li, J. Wang, J. C. Yu and C.-H. Yan, Plasmonic harvesting of light energy of Suzuki coupling reactions, *J. Am. Chem. Soc.*, 2013, **135**, 5588.
44 B. D. Ravetz, N. E.-S. Tay, C. L. Joe, M. Sezen-Edmonds, M. A. Schmidt, Y. Tan, J. M. Janey, M. D. Eastgate and T. Rovis, Development of a platform for near-infrared photoredox catalysis, *ACS Cent. Sci.*, 2020, **6**, 2053.
45 C. Kütahya, Y. Yagci and B. Strehmel, Near-infrared photoinduced copper-catalyzed azide-alkyne click chemistry with a cyanine comprising a barbiturate group, *ChemPhotoChem*, 2019, **3**, 1180.
46 A. R.-O. Kosso, N. Sellet, A. Baralle, M. Cormier and J.-P. Goddard, Cyanine-based near infra-red organic photoredox catalysis, *Chem. Sci.*, 2021, **12**, 6964.
47 N. Sellet, M. Cormier and J.-P. Goddard, The dark side of photocatalysis: near-infrared photoredox catalysis for organic synthesis, *Org. Chem. Front.*, 2021, **8**, 6783.
48 J. C. Wedal and W. J. Evans, A rare-earth metal retrospective to stimulate all fields, *J. Am. Chem. Soc.*, 2021, **143**, 18354.
49 M. Shibasaki, K. Yamada and N. Yoshikawa, in *Lewis Acids in Organic Synthesis*, ed. H. Yamamoto, Wiley-VCH, Weinheim, 2000, ch. 20, pp. 911–944.
50 J. A. Cotruvo, Jr., The chemistry of lanthanides in biology: recent discoveries, emerging principles, and technological applications, *ACS Cent. Sci.*, 2019, **5**, 1496.

Open Access Article. Published on 13 2022. Downloaded on 28.01.2026 17:57:53.
This article is licensed under a Creative Commons Attribution-NonCommercial 3.0 Unported Licence.

51 S. Fukuzumi, J. Jung, Y.-M. Lee and W. Nam, Effects of Lewis acids on photoredox catalysis, *Asian J. Org. Chem.*, 2017, **6**, 397.
52 H. Pellissier, Recent developments in enantioselective lanthanide-catalyzed transformations, *Coord. Chem. Rev.*, 2017, **336**, 96.
53 Z. Hu and D. Zhao, Metal–organic frameworks with Lewis acidity: synthesis, characterization, and catalytic applications, *CrystEngComm*, 2017, **19**, 4066.
54 C. Song, Z. Wang, Z. Yin, D. Xiao and D. Ma, Principles and applications of photothermal catalysis, *Chem. Catal.*, 2022, **2**, 1.
55 C. Chen, Y. Kuang and L. Hu, Challenges and opportunities for solar evaporation, *Joule*, 2019, **3**, 683.
56 M. Gao, L. Zhu, C. K. Peh and G. W. Ho, Solar absorber material and system designs for photothermal water vaporization towards clean water and energy production, *Energy Environ. Sci.*, 2019, **12**, 841.
57 S. Link, C. Burda, B. Nikoobakht and M. A. El-Sayed, Laser-induced shape changes of colloidal gold nanorods using femtosecond and nanosecond laser pulses, *J. Phys. Chem. B*, 2000, **104**, 6152.
58 K. M. Haas and B. J. Lear, Billion-fold rate enhancement of urethane polymerization via the photothermal effect of plasmonic gold nanoparticles, *Chem. Sci.*, 2015, **6**, 6462.
59 M. Kim, J.-H. Lee and J.-M. Nam, Plasmonic photothermal nanoparticles for biomedical applications, *Adv. Sci.*, 2019, **6**, 1900471.
60 Q. Tian, F. Jiang, R. Zou, Q. Liu, Z. Chen, M. Zhu, S. Yang, J. Wang, J. Wang and J. Hu, Hydrophilic Cu_9S_5 nanocrystals: a Photothermal agent with a 25.7% heat conversion efficiency for photothermal ablation of cancer cells *in Vivo*, *ACS Nano*, 2011, **5**, 9761.
61 S. Ariyasu, J. Mu, X. Zhang, Y. Huang, E. K.-L. Yeow, H. Zhang and B. Xing, Investigation of thermally induced cellular ablation and heat response triggered by planar MoS_2-based nanocomposite, *Bioconjugate Chem.*, 2017, **28**, 1059.
62 M.-C. Wu, A. R. Deokar, J.-H. Liao, P.-Y. Shih and Y.-C. Ling, Graphene-based photothermal agent for rapid and effective killing of bacteria, *ACS Nano*, 2013, **7**, 1281.
63 L. Xiao, X. Chen, X. Yang, J. Sun and J. Geng, Recent advances in polymer-based photothermal materials for biological applications, *ACS Appl. Polym. Mater.*, 2020, **2**, 4273.
64 T. D. Cong, Z. Wang, M. Hu, Q. Han and B. Xing, Extra-specific manifestation of nanoheater's position effect on distinctive cellular photothermal responses, *ACS Nano*, 2020, **14**, 5836.
65 K. Zhao, J. Sun, F. Wang, A. Song, K. Liu and H. Zhang, Lanthanide-based photothermal materials: fabrication and biomedical applications, *ACS Appl. Bio Mater.*, 2020, **3**, 3975.
66 A. Gupta, S. Ghosh, M. K. Thakur, J. Zhou, K. Ostrikov, D. Ji and S. Chattopadhyay, Up-conversion hybrid nanomaterials for light- and heat-driven applications, *Prog. Mater. Sci.*, 2021, **121**, 100838.
67 D. Jaque, L. M. Maestro, B. del Rosal, P. Haro-Gonzalez, A. Benayas, J. L. Plaza, E. M. Rodríguez and J. G. Solé, Nanoparticles for photothermal therapies, *Nanoscale*, 2014, **6**, 9494.
68 X. Y. Wu and E. K.-L. Yeow, Tuning the NIR downconversion luminescence and photothermal conversion efficiencies of $MNd_xY_{1-x}F_4$ (M = Na and Li) nanocrystals for use in anti-counterfeiting labels with opposite displays, *Nanoscale*, 2019, **11**, 15259.
69 L. Marciniak, A. Pilch, S. Arabasz, D. Jin and A. Bednarkiewicz, Heterogeneously Nd^{3+} doped single nanoparticles for NIR-induced heat conversion, luminescence, and thermometry, *Nanoscale*, 2017, **9**, 8288.
70 U. Rocha, K. U. Kumar, C. Jacinto, J. Ramiro, A. J. Caamaño, J. G. Solé and D. Jaque, Nd^{3+} doped LaF_3 nanoparticles as self-monitored photo-thermal agents, *Appl. Phys. Lett.*, 2014, **104**, 053703.
71 Q. Shao, Z. Yang, G. Zhang, Y. Hu, Y. Dong and J. Jiang, Multifunctional lanthanide-doped core/shell nanoparticles: integration of upconversion luminescence, temperature sensing, and photothermal conversion properties, *ACS Omega*, 2018, **3**, 188.
72 E. C. Ximendes, U. Rocha, K. U. Kumar, C. Jacinto and D. Jaque, LaF_3 core/shell nanoparticles for subcutaneous heating and thermal sensing in the second biological-window, *Appl. Phys. Lett.*, 2016, **108**, 253103.
73 D. Mateo, J. L. Cerrillo, S. Durini and J. Gascon, Fundamentals and applications of photo-thermal catalysis, *Chem. Soc. Rev.*, 2021, **50**, 2173.
74 X. Xie, N. Gao, R. Deng, Q. Sun and Q.-H. Xu, X. Liu. Mechanistic investigation of photon upconversion in Nd^{3+}-sensitized core-shell nanoparticles, *J. Am. Chem. Soc.*, 2013, **135**, 12608.
75 R. Deng, F. Qin, R. Chen, W. Huang, M. Hong and X. Liu, Temporal full-colour tuning through non-steady-state upconversion, *Nat. Nanotechnol.*, 2015, **10**, 237.
76 Y. Ji, W. Xu, N. Ding, H. Yang, H. Song, Q. Liu, H. Ågren, J. Widengren and H. Liu, Huge upconversion luminescence enhancement by a cascade optical field modulation strategy facilitating selective multispectral narrow-band near-infrared photodetection, *Light: Sci. Appl.*, 2020, **9**, 184.
77 Q. Li, S. Yuan, F. Liu, X. Zhu and J. Liu, Lanthanide-doped nanoparticles for near-infrared light activation of photopolymerization: fundamentals, optimization and applications, *Chem. Rec.*, 2021, **21**, 1681.
78 Z. Chen, X. Wang, S. Li, S. Liu, H. Miao and S. Wu, Near-infrared light driven photopolymerization based on photon upconversion, *ChemPhotoChem*, 2019, **3**, 1077.
79 K. Wang, J. Peña and J. Xing, Upconversion nanoparticle-assisted photopolymerization, *Photochem. Photobiol.*, 2020, **96**, 741.
80 A. Stepuk, D. Mohna, R. N. Grass, M. Zehnde, K. W. Krämer, F. Pellé, A. Ferrier and W. J. Stark, Use of NIR light and upconversion phosphors in light-curable polymers, *Dent. Mater.*, 2012, **28**, 304.
81 R. Liu, H. Chen, Z. Li, F. Shi and X. Liu, Extremely deep photopolymerization using upconversion particles as internal lamps, *Polym. Chem.*, 2016, **7**, 2457.

Open Access Article. Published on 13 2022. Downloaded on 28.01.2026 17:57:53.
This article is licensed under a Creative Commons Attribution-NonCommercial 3.0 Unported Licence.

82 R. Popielarz and O. Vogt, Effect of coinitiator type on initiation efficiency of two-component photoinitiator systems based on eosin, *J. Polymer Sci., Part A*, 2008, **46**, 3519.
83 Q. Xiao, Y. Ji, Z. Xiao, Y. Zhang, H. Lin and Q. Wang, Novel multifunctional $NaYF_4$:Er^{3+},Yb^{3+}/PEGDA hybrid microspheres: NIR-light-activated photopolymerization and drug delivery, *Chem. Commun.*, 2013, **49**, 1527.
84 S. Beyazit, S. Ambrosini, N. Marchyk, E. Palo, V. Kale, T. Soukka, B. T.-S. Bui and K. Haupt, Versatile synthetic strategy for coating upconverting nanoparticles with polymer shells through localized photopolymerization by using the particles as internal light sources, *Angew. Chem., Int. Ed.*, 2014, **53**, 8919.
85 A. Kocaarslan, S. Tabanli, G. Eryurek and Y. Yagci, Near-infrared free-radical and free-radical-promoted cationic photopolymerizations by in-source lighting using upconverting glass, *Angew. Chem., Int. Ed.*, 2017, **56**, 14507.
86 P. Lederhose, Z. Chen, R. Müller, J. P. Blinco, S. Wu and C. Barner-Kowollik, Near-infrared photoinduced coupling reactions assisted by upconversion nanoparticles, *Angew. Chem., Int. Ed.*, 2016, **55**, 12195.
87 Z. Li, X. Zou, F. Shi, R. Liu and Y. Yagci, Highly efficient dandelion-like near-infrared light photoinitiator for free radical and thiol-ene photopolymerizations, *Nat. Commun.*, 2019, **10**, 3560.
88 X. Meng, H. Lu, Z. Li, C. Wang, R. Liu, X. Guan and Y. Yagci, Near-infrared light induced cationic polymerization based on upconversion and ferrocenium photochemistry, *Polym. Chem.*, 2019, **10**, 5574.
89 Z. Li, J. Zhu, X. Guan, R. Liu and Y. Yagci, Near-infrared-induced cationic polymerization initiated by using upconverting nanoparticles and titanocene, *Macromol. Rapid Commun.*, 2019, **40**, 1900047.
90 W. Zhang, J. He, C. Lv, Q. Wang, X. Pang, K. Matyjaszewski and X. Pan, Atom transfer radical polymerization driven by near-infrared light with recyclable upconversion nanoparticles, *Macromolecules*, 2020, **53**, 4678.
91 L. Hu, Q. Hao, L. Wang, Z. Cui, P. Fu, M. Liu, X. Qiao and X. Pang, The in situ ''grafting from'' approach for the synthesis of polymer brushes on upconversion nanoparticles via NIR-mediated RAFT polymerization, *Polym. Chem.*, 2021, **12**, 545.
92 C. Ding, J. Wang, W. Zhang, X. Pan, Z. Zhang, W. Zhang, J. Zhu and X. Zhu, Platform of near-infrared light-induced reversible deactivation radical polymerization: upconversion nanoparticles as internal light sources, *Polym. Chem.*, 2016, **7**, 7370.
93 D. Oprych and B. Strehmel, Mediated generation of conjugate acid by UV and blue sensitizers with upconversion nanoparticles at 980 nm, *Chem. – Eur. J.*, 2021, **27**, 4297.
94 X. Zou, J. Zhu, P. Hu and R. Liu, Methods to evaluate near-infrared photoinitiating systems for photopolymerisation reactions assisted by upconversion materials, *ChemPhotoChem*, 2021, **5**, 915.
95 X. Kang, W. Shang, Q. Zhu, J. Zhang, T. Jiang, B. Han, Z. Wu, Z. Li and X. Xing, Mesoporous inorganic salts with crystal defects: unusual catalysts and catalyst supports, *Chem. Sci.*, 2015, **6**, 1668.
96 B. Yu, E. Hao, S. Fang, Z. Liu, Y. Wang, Z. Lv, N. Li, X. Zhang, L. Shi and Y. Du, Controlled synthesis of high quality scandiumbased nanocrystals as promising recyclable catalysts for silylcyanation reaction, *Nanoscale*, 2017, **9**, 10987.
97 A. Astruc, S. Célérier, E. Pavon, A.-S. Mamede, L. Delevoye and S. Brunet, Mixed $Ba_{1-x}La_xF_{2+x}$ fluoride materials as catalyst for the gas phase fluorination of 2-chloropyridine by HF, *Appl. Catal., B*, 2017, **204**, 107.
98 T. Li, Q. Chen, J. Yu, J. Xia, Y. Li, K. Xu, Y. Luo, Q. Liu and H. Guo, YF_3: a nanoflower-like catalyst for efficient nitrogen fixation to ammonia under ambient conditions, *Catal. Sci. Technol.*, 2021, **11**, 6750.
99 A. Bednarkiewicz, D. Wawrzynczyk, M. Nyk and W. Strek, Optically stimulated heating using Nd^{3+} doped $NaYF_4$ colloidal near infrared nanophosphors, *Appl. Phys. B*, 2011, **103**, 847.
100 A. Bednarkiewicz, D. Wawrzynczyk, M. Nyk and W. Strek, Synthesis and spectral properties of colloidal Nd^{3+} doped $NaYF_4$ nanocrystals, *Opt. Mater.*, 2011, **33**, 1481.
101 A.-R. Hong, J. Y. Byun, K. Lee and H. S. Jang, Sub-20 nm $LiErF_4$-based upconversion nanophosphors for simultaneous imaging and photothermal therapeutics, *ACS Appl. Nano Mater.*, 2020, **3**, 8662.
102 B. Liu, C. Li, P. Yang, Z. Hou and J. Lin, 808-nm-light-excited lanthanide-doped nanoparticles: rational design, luminescence control and theranostic applications, *Adv. Mater.*, 2017, **29**, 1605434.
103 S. T. Dibaba, X. Ge, W. Ren and L. Sun, Recent progress of energy transfer and luminescence intensity boosting mechanism in Nd^{3+}-sensitized upconversion nanoparticles, *J. Rare Earths*, 2019, **37**, 791.
104 V. K. Tikhomirov, K. Driesen, V. D. Rodriguez, P. Gredin, M. Mortier and V. V. Moshchalkov, Optical nanoheater based on the Yb^{3+}–Er^{3+} co-doped nanoparticles, *Opt. Express*, 2009, **17**, 11794.
105 X. Zhao, H. Suo, Z. Zhang and C. Guo, Upconverting CeO_2: Yb^{3+}/Tm^{3+} hollow nanospheres for photo-thermal sterilization and deep-tissue imaging in the first biological window, *Ceram. Int.*, 2019, **45**, 21910.
106 X. Huang and M. A. El-Sayed, in *Nanotechnology in Biology and Medicine Methods, Devices, and Applications*, ed. T. Vo-Dinh, Taylor & Francis Group, Boca Raton, 2nd edn, 2018, ch. 28, pp. 627–650.
107 X. Y. Wu, J. Y. Tham, A.-M. Chacko and E. K.-L. Yeow, The role of ligand acid–base reaction in the facile synthesis of alkali metal neodymium penta- and heptafluoride nanocrystals, *Chem. Mater.*, 2021, **33**, 8367.
108 X. Y. Wu and E. K.-L. Yeow, Ultrathin near-infrared light activated nano-hotplate catalyst, *Small*, 2020, **16**, 2002698.
109 L. Ding, F. Ren, Z. Liu, Z. Jiang, B. Yun, Q. Sun and Z. Li, Size-dependent photothermal conversion and photoluminescence of theranostic $NaNdF_4$ nanoparticles under excitation of differentwavelength lasers, *Bioconjugate Chem.*, 2020, **31**, 340.

Open Access Article. Published on 13 2022. Downloaded on 28.01.2026 17:57:53.
This article is licensed under a Creative Commons Attribution-NonCommercial 3.0 Unported Licence.

110 L. Xu, J. Li, K. Lu, S. Wen, H. Chen, M. K. Shahzad, E. Zhao, H. Li, J. Ren, J. Zhang and L. Liu, Sub-10 nm $NaNdF_4$ nanoparticles as near-infrared photothermal probes with self-temperature feedback, *ACS Appl. Nano Mater.*, 2020, **3**, 2517.

111 H. Jia, Z. Liu, L. Liao, Y. Gu, C. Ding, J. Zhao, W. Zhang, X. Hu, X. Feng, Z. Chen, X. Liu and J. Qiu, Upconversion luminescence from Ln^{3+}(Ho^{3+}, Pr^{3+}) ion-doped $BaCl_2$ particles via NIR light of sun excitation, *J. Phys. Chem. C*, 2018, **122**, 9606.

112 D. Cambié, J. Dobbelaar, P. Riente, J. Vanderspikken, C. Shen, P. H. Seeberger, K. Gilmore, M. G. Debije and T. Noël, Energy-efficient solar photochemistry with luminescent solar concentrator based photomicroreactors, *Angew. Chem., Int. Ed.*, 2019, **131**, 14512.

113 T. Sheng, M. Xu, Q. Li, Y. Wu, J. Zhang, J. Liu, X. Zhu and Y. Zhang, Elucidating the role of energy management in making brighter, and more colorful upconversion nanoparticles, *Mater. Today Phys.*, 2021, **20**, 100451.

114 H.-X. Mai, Y.-W. Zhang, R. Si, Z.-G. Yan, L.-D. Sun, L.-P. You and C.-H. Yan, High-quality sodium rare-earth fluoride nanocrystals: controlled synthesis and optical properties, *J. Am. Chem. Soc.*, 2006, **128**, 6426.

115 A. Gee and X. Xu, Surface functionalization of upconversion nanoparticles with different moieties for biomedical applications, *Surfaces*, 2018, **1**, 96.

116 A. Dong, X. Ye, J. Chen, Y. Kang, T. Gordon, J. M. Kikkawa and C. B. Murray, A generalized ligand-exchange strategy enabling sequential surface functionalization of colloidal nanocrystals, *J. Am. Chem. Soc.*, 2011, **133**, 998.

117 H. Dong, L.-D. Sun and C.-H. Yan, Local structure engineering in lanthanide-doped nanocrystals for tunable upconversion emissions, *J. Am. Chem. Soc.*, 2021, **143**, 20546.

118 Z. Yu, W. Hu, H. Zhao, X. Miao, Y. Guan, W. Cai, Z. Zeng, Q. Fan and T. T.-Y. Tan, Generating new cross-relaxation pathways by coating Prussian blue on $NaNdF_4$ to fabricate enhanced photothermal agents, *Angew. Chem., Int. Ed.*, 2019, **58**, 8536.

119 X. Wang, H. Li, F. Li, X. Han and G. Chen, Prussian blue-coated lanthanide-doped core/shell/shell nanocrystals for NIR-II image-guided photothermal therapy, *Nanoscale*, 2019, **11**, 22079.

120 Y. Wu, J. Xu, X. Qin, J. Xu and X. Liu, Dynamic upconversion multicolour editing enabled by molecule-assisted optoelectrochemical modulation, *Nat. Commun.*, 2021, **12**, 2022.

121 R. G. Geitenbeek, A.-E. Nieuwelink, T. S. Jacobs, B. B.-V. Salzmann, J. Goetze, A. Meijerink and B. M. Weckhuysen, In situ luminescence thermometry to locally measure temperature gradients during catalytic reactions, *ACS Catal.*, 2018, **8**, 2397.

122 A. M. Kaczmarek, H. S. Jena, C. Krishnaraj, H. Rijckaert, S. K.-P. Veerapandian, A. Meijerink and P. Van Der Voort, Luminescent ratiometric thermometers based on a 4f–3d grafted covalent organic framework to locally measure temperature gradients during catalytic reactions, *Angew. Chem., Int. Ed.*, 2021, **60**, 3727.

123 C. Krishnaraj, H. Rijckaert, H. S. Jena, P. Van Der Voort and A. M. Kaczmarek, Upconverting Er^{3+}–Yb^{3+} inorganic/covalent organic framework core–shell nanoplatforms for simultaneous catalysis and nanothermometry, *ACS Appl. Mater. Interfaces*, 2021, **13**, 47010.

124 G. Jalani, V. Tam, F. Vetrone and M. Cerruti, Seeing, targeting and delivering with upconverting nanoparticles, *J. Am. Chem. Soc.*, 2018, **140**, 10923.

125 A. Gnach, T. Lipinski, A. Bednarkiewicz, J. Rybka and J. A. Capobianco, Upconverting nanoparticles: assessing the toxicity, *Chem. Soc. Rev.*, 2015, **44**, 1561.

126 M. Nyk, R. Kumar, T. Y. Ohulchanskyy, E. J. Bergey and P. N. Prasad, High contrast in vitro and in vivo photoluminescence bioimaging using near infrared to near infrared up-conversion in Tm^{3+} and Yb^{3+} doped fluoride nanophosphors, *Nano Lett.*, 2008, **8**, 3834.

127 A. Lay, O. H. Sheppard, C. Siefe, C. A. McLellan, R. D. Mehlenbacher, S. Fischer, M. B. Goodman and J. A. Dionne, Optically robust and biocompatible mechanosensitive upconverting nanoparticles, *ACS Cent. Sci.*, 2019, **5**, 1211.

128 H. Oliveira, A. Bednarkiewicz, A. Falk, E. Fröhlich, D. Lisjak, A. Prina-Mello, S. Resch, C. Schimpel, I. V. Vrček, E. Wysokińska and H. H. Gorris, Critical considerations on the clinical translation of upconversion nanoparticles (UCNPs): recommendations from the European upconversion network (COST Action CM1403), *Adv. Healthcare Mater.*, 2019, **8**, 1801233.

129 A. Hischemöller, J. Nordmann, P. Ptacek, K. Mummenhoff and M. Haase, In-vivo imaging of the uptake of upconversion nanoparticles by plant roots, *J. Biomed. Nanotechnol.*, 2009, **5**, 278.

130 X. Xu, W. Li, C. Hu, B. Lei, X. Zhang, Y. Li, Q. Zhan, Y. Liu and J. Zhuang, Promoting the growth of mung bean plants through uptake and light conversion of $NaYF_4$:Yb,Er@CDs nanocomposites, *ACS Sustainable Chem. Eng.*, 2020, **8**, 9751.